Stony Brook University

Determining Ligand-Binding Induced Conformational Changes in H-NOX Domains

A Thesis Presented

by

Farzan Mirza Gorgani

to

The Graduate School

in Partial Fulfillment of the

Requirements

for the Degree of

Master of Science

in

Chemistry

Stony Brook University

December 2010

Stony Brook University

The Graduate School

Farzan Mirza Gorgani

We, the thesis committee for the above candidate for the

Master of Science degree, hereby recommend

acceptance of this thesis.

Elizabeth M. Boon, Ph.D., Thesis Advisor
Professor, Department of Chemistry

Robert C. Rizzo, Ph.D., Chairperson of Defense
Professor, Department of Applied Mathematics and Statistics

Joseph W. Lauher, Ph.D., Third Member
Professor, Department of Chemistry

This thesis is accepted by the Graduate School

Lawrence Martin
Dean of the Graduate School

Stony Brook University

Abstract of Thesis

Determining Ligand-Binding Induced Conformational Changes in H-NOX Domains

by

Farzan Mirza Gorgani

Master of Science

in

Chemistry

Stony Brook University

2010

Nitric Oxide (NO) has diverse and important roles in prokaryote and eukaryote biology. In addition to its role as a powerful toxin used to kill pathogens and tumor cells, NO also functions as a signaling molecule that mediates mechanisms such as vasodilatation, neurotransmission and biofilm formation. Our objective is to elucidate the role of NO in bacterial biofilm formation. Due to their resistance to antibiotics, biofilms are known to plague hospitals and immune compromised patients. As a first step in this objective, we are interested in characterizing the bacterial NO sensor Heme-Nitric oxide/OXygen binding domain (H-NOX). We predict that H-NOX changes its conformation upon binding nitric oxide (NO) and this causes changes in its interactions with downstream effectors, leading ultimately to biofilm formation. Here we describe our efforts towards the use of fluorescent resonance energy transfer (FRET) and computational modeling to determine conformational changes in H-NOX that take place upon ligand binding. The unnatural fluorescent amino acid p-cyanophenylalanine was

incorporated into the H-NOX of *S. woodyi* for use in FRET studies. Furthermore, computational simulations using AMBER force field tools were carried out in the H-NOX domain from *T. tengcongensis*. Root mean square deviation (RMSD) values of the amino acid backbone, certain helices, and dihedral angels of the heme were measured. Characterizing ligand-induced conformational changes in H-NOX will aid in further understanding of the role of NO in biofilm formation. Better understanding of biofilm formation will ultimately lead to strategies to eliminate them.

Table of Contents

List of Figures

List of Abbreviations

Nitric oxide, NO; Nitric Oxide Synthase, NOS; Soluble guanylate cyclase, sGC; Guanosine triphosphate, GTP; Cyclic guanosine monophosphate, cGMP; Heme-Nitric oxide/OXygen binding protein, H-NOX; Diguanylate cyclase, DGC; bis-(3',5')-cyclic dimeric guanosine monophosphate, c-di-GMP; Extracellular polysaccharide, EPS; *Shewanella woodyi, S. woodyi, Sw*; Fluorescent (Förster) Resonance Energy Transfer, FRET; Enhanced cyan fluorescent protein, ECYP; Enhanced yellow fluorescent protein, EYFP; *p*-Cyanophenylalanine, pCN; Förster distance, R_o; *Thermoanaerobacter tengcongensis, Tt*; Proline, P; Tyrosine, Y; Histidine, H; Alaline, A; Tryptophan, W; Leucine, L; Phenylalanine, F; Valine, V; Nuclear magnetic resonance, NMR; Luria Broth, LB; Wild-type, wt; Milliliters, mL; Micrograms, μg; Rotations per minute, rpm; Microliter, μL; Trifluoroacetic acid, TFA; Matrix-assisted laser desorption/ionization-time of flight, MALDI-TOF; Institute of Chemical Biology and Drug Discovery, ICBⅅ Ultraviolet/Visible, UV-Vis; Millimeter, mm; Root mean square deviation, RMSD; Molecular dynamics, MD; Nanosecond, ns

Chapter 1: Background Information

1.1 Nitric Oxide

In the 1980's, Dr. Robert Furchgott of SUNY Downstate Medical Center found that the causative agent of smooth muscle relaxation was neither organic nor an ion, but a gas[1]. This gas was Nitric Oxide (NO), a diatomic gas molecule that was recently discovered to be a first messenger in several eukaryotic and prokaryote signaling pathways[2]. NO has diverse and important roles in prokaryote and eukaryote biology. In addition to its role as a powerful toxin used to kill pathogens and tumor cells, NO also functions as a signaling molecule that mediates mechanisms such as vasodilatation, neurotransmission, and platelet aggregation[3,4,5]. The most well known NO pathway is the mammalian vasodilatation pathway as illustrated by Figure 1-1.

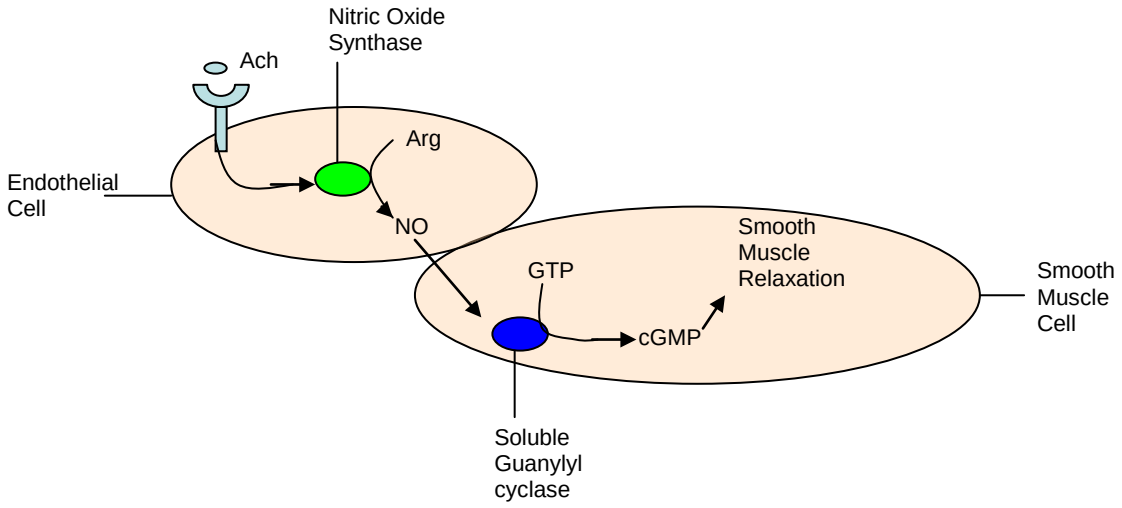

Figure 1-1. Vasodilatation pathway in mammals.

Acetylcholine (Ach) binding to receptors on smooth muscle endothelium cells causes NO to be formed from arginine (Arg) by Nitric Oxide Synthase (NOS). NO binds to a heme-containing domain on soluble guanylyl cyclase (sGC), which activates the

cyclase domain and converts guanosine triphosphate (GTP) into cyclic guanosine monophosphate (cGMP). This increase in cGMP causes smooth muscle relaxation[6].

1.2 H-NOX

Prokaryotes code for NO sensors homologous to the heme domain from sGC. These NO sensors do not lead to smooth muscle relaxation, but have other downstream effects. The prokaryotic homolog of sGC's heme binding domain is, usually, a standalone protein called Heme-Nitric oxide/OXygen binding domain (H-NOX)[7] with a bacterial di-guanylate cyclase or histidine kinase protein in the same putative operon. Di-guanylyl cyclases (DGC) convert 2 molecules of GTP into the common bacterial second messenger cyclic di-GMP (c-di-GMP). We have shown that H-NOX interacts with DGC (ref Niu, Saj, Tanaya unpublished work) and that H-NOX has an extremely high affinity for NO[7-10]. Thus, we hypothesize that when NO binds H-NOX, it changes its conformation, leading to a change in its interaction with DGC, ultimately leading to regulation of the conversion of GTP into c-di-GMP (Figure 1-2).

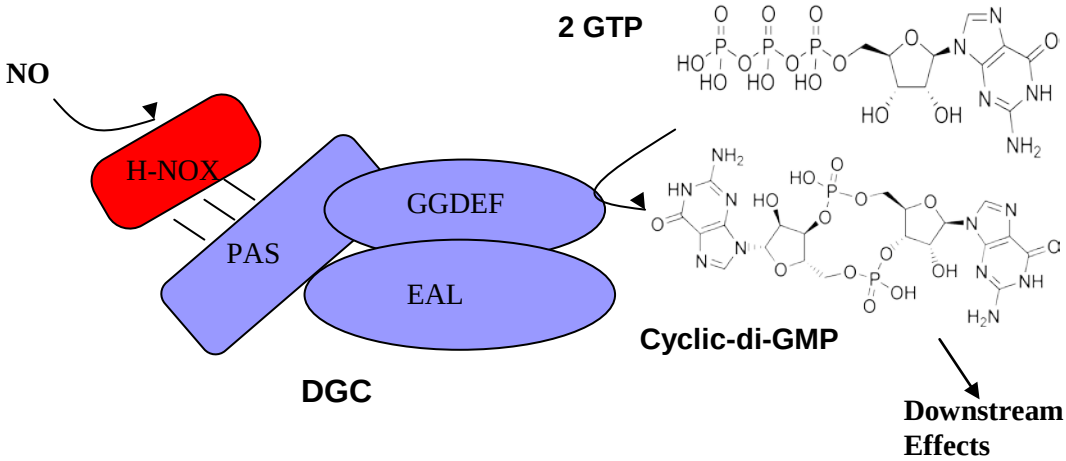

Figure 1-2. Upon binding to NO, H-NOX is thought to interact with DGC. DGC has three known domain, PAS, GGDEF and EAL. The PAS domain is thought to interact with H-NOX. The GGDEF domain converts 2 GTP into c-di-GMP. The EAL domain converts c-di-GMP into 2 GMP.

1.3 Biofilms

Increasing levels of c-di-GMP in certain bacterial species has been shown to effect biofilm formation[11]. Biofilms are communities of bacteria that secrete a thick extracellular polysaccharide (EPS) matrix. Specifically, increased c-di-GMP concentrations increase EPS production, leading to an increase in biofilm thickness. In a process called quorum sensing, bacteria can communicate with each other using small molecule signals and through this communication, they can detect the density of cells around them. Once the density of cells become appropriate, the bacteria begin to colonize and start biofilming as illustrated in Figure 1-3.

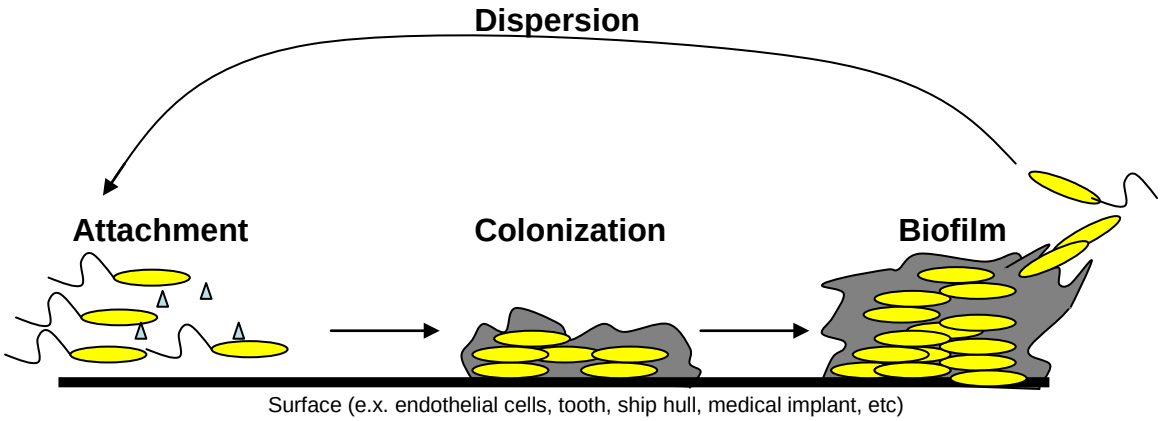

Figure 1-3. Bacterial cells can detect the density of cells around them through quorum sensing signals (green triangles). Once the density is appropriate, they can then colonize and start secreting polysaccharides to form biofilms.

Biofilms are known to plague hospitals and immune compromised patients because of their antibiotic resistance. The polysaccharide shell serves as a physical barrier that prevents antibiotic molecules from reaching the cells. This has significant consequences: for example, the most common cause of death of cystic fibrosis patents is succumbing to the antibiotic resistant biofilms of *Pseudomonas aeruginosa.* Biofilms can also infect water supplies, medical implants and hospital lines, cause plaque on teeth, and

degrade the steel on ship hulls. Because of their vast significance, understanding biofilm formation is extremely important.

1.4 *Shewanella Woodyi*

Shewanella Woodyi (*Sw*) is a marine proteobacterium that contains a conserved H-NOX gene (gi: 170727096) with a diguanylate cyclase gene (DGC; gi: 170727095) downstream in the same putative operon. It has been shown that *Sw*DGC and c-di-GMP are involved in biofilm formation[11], cell motility[12,13] and that NO can mediate biofilm formation in other bacterial species[19]. Since we know that *Sw*H-NOX tightly binds NO and interacts with SwDGC[11], we predict that it is arbiter in this pathway. For reasons explained below, we will use the *Sw*H-NOX in our fluorescent experiments to help determine the change in conformation upon NO binding.

1.5 Fluorescent (Förster) Resonance Energy Transfer and *p*-Cyanophenylalanine

Fluorescent (Förster) Resonance Energy Transfer (FRET) is a method in which nanoscale distances between fluorophores are measured. Excitation energy can be transferred from one fluorescent group (donor) to another fluorescent group (acceptor) as long as they are in very close proximity. The efficiency of transfer between the two fluorescent groups that are bound to sites on a protein decreases sharply as the distance between the two groups increases, therefore allowing for a measure of distance changes in a process. FRET is most commonly performed to determine whether two proteins are interacting with one another. As illustrated in Figure 1-4, enhanced cyan fluorescent protein (ECFP) is labeled to the first protein and enhanced yellow fluorescent protein (EYFP) is labeled on the other. As the proteins interact, emission at 480nm is no longer

detected but 535nm is. This suggests that ECFP had "transferred" its energy to EYFP because they, and therefore the two proteins, are in close proximity[18].

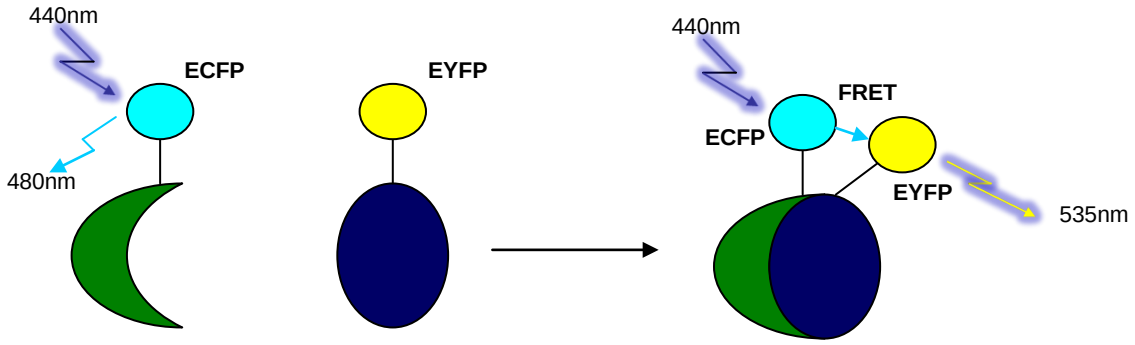

Figure 1-4. FRET between ECFP and EYFP as the proteins they are labeled to interact with each other.

p-Cyanophenylalanine (pCN; Figure 1-5) is an unnatural amino acid that will be used as a fluorescent donor in our FRET experiments. As opposed to other fluorphores, pCN is very small, about the size of tyrosine, which means that it may not interfere with native protein structures as a larger fluorophore would. In addition, pCN has a small Förster distance, R_o (distance at which the energy transfer efficiency is 50%), of 16Å which allows for measurements of intramolecular movement. Larger fluorophores used in intermolecular movement have larger R_o values because the distances are relatively larger. pCN can be selectively excited at 240nm and has an emission maximum of 290nm. pCN can be used in FRET when paired with tryptophan to measure intramolecular distances and therefore changes in protein conformation[14].

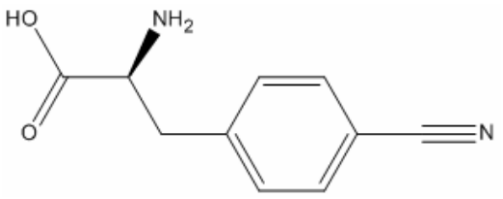

Figure 1-5. *p*-Cyanophenylalanine.

1.6 *Thermoanaerobacter tengcongensis*

Thermoanaerobacter tengcongensis (*Tt*) is a thermophilic bacterium first isolated from hot springs in Tengcong, China[15]. *Tt* contains an H-NOX domain, homologous to sGC, which is fused to a predicted methyl-accepting chemotaxis protein domain[16] (gi: 20807169). *Tt*H-NOX has the ability, as opposed to *Sw*H-NOX, to bind oxygen due to the presence of a distal tyrosine140 that hydrogen bonds and stabilizes molecular oxygen. The crystal structure of this member of the H-NOX family has been solved to 1.77Å bound to molecular oxygen (PDB ID: 1U4H, chain A; Figure 1-6)[16]. One of the most distinct and interesting features of the H-NOX class of proteins, as determined from this structure, is that the heme is not planar, but is extremely distorted due to the presence of proline 115 in the heme pocket (Figure 1-7).

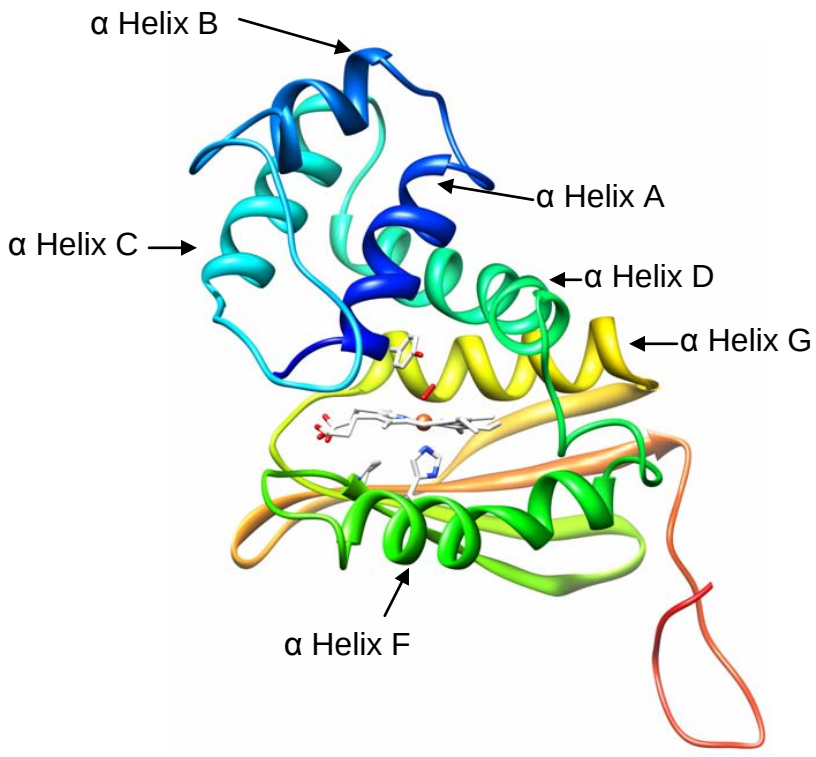

Figure 1-6. Crystal structure of *Tt*H-NOX. Y140, H102 and P115 are shown explicitly (PDB ID: 1U4H, chain A).

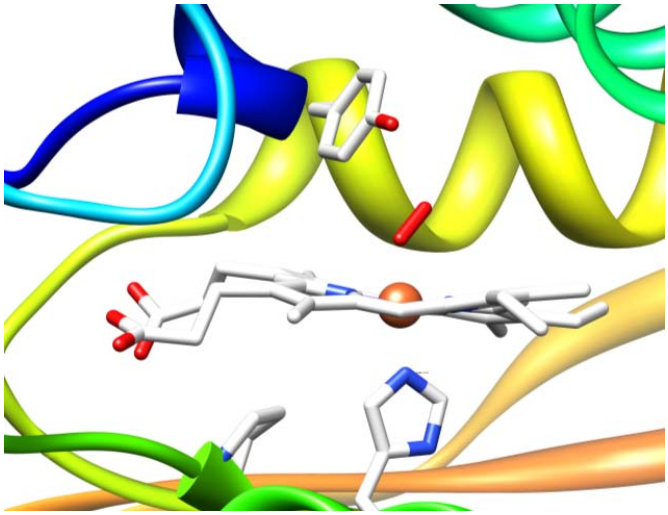

Figure 1-7. Close up of the heme environment of *Tt*H-NOX.

The heme distortion is caused by van der Waals interactions with Proline115. Sequence alignments have shown that P115 is conserved throughout the H-NOX family, suggesting that this heme distortion is conserved and is important for function. It had been previously hypothesized that the P115A mutant would relieve the ring strain and mimic the active, NO bound, state[17]. The P115A mutant bound to molecular oxygen was crystallized and the structure was solved to 2.12Å (PDB ID: 3EEE, chain C)[8]. The P115A mutant is shown below in Figure 1-8 along with a close up of its heme environment, Figure 1-9.

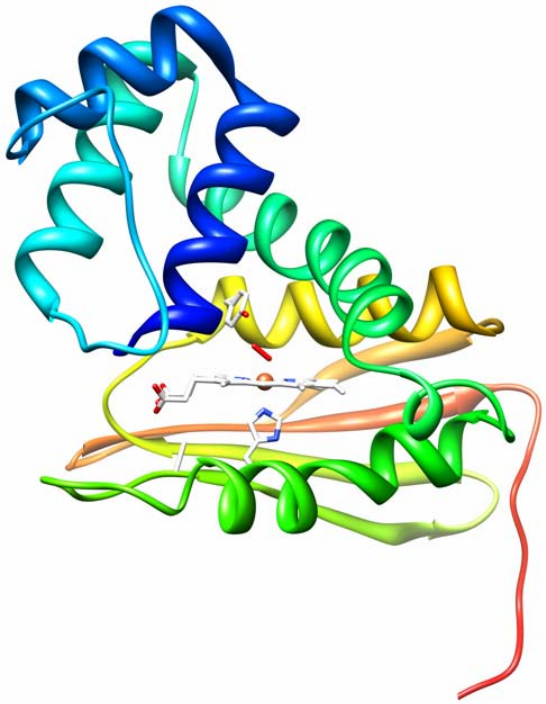

Figure 1-8. P115A mutant of *Tt*H-NOX. Y140, H102 and A115 are shown explicitly (PDB ID: 3EEE, chain C).

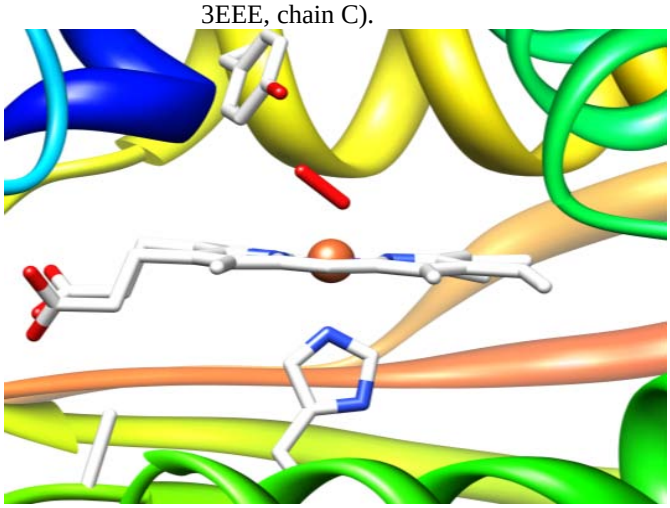

Figure 1-9. Close up of the heme environment of P115A *Tt*H-NOX.

When comparing Figures 1-7 and 1-9, it can be seen that the P115A mutant adopts a much flatter heme structure.

1.7 Computational Simulations

Computational simulation is a very powerful tool as it can reproduce laboratory experiments and enlighten us on protein motion. Conformational changes in proteins are extremely important to understand because it is these changes that allow proteins to

perform certain acts, whether its catalysis, protein-protein interactions, facilitated diffusion, etc. Crystal structure or NMR coordinates, along with several other parameters, are given to molecular mechanics force field programs which can then calculate trajectories in a given time scale. These trajectories are the predicted motions of the protein and can be used to interpret their function.

1.8 References

1. Koshlan, D.E. “The Molecule of the Year” *Science.* **1992,** 258, 5090, 1861.

2. Culotta, E., Koshlan, D.E. “NO news is Good News” *Science.* **1992,** 258, 5090, 1862-1865.

3. Toda, N., Okamura, T. “The pharmacology of nitric oxide in the peripheral nervous system of blood vessels.” *Pharmacol.* **2003,** *Rev.* 55, 271-324.

4. Hare, J.M., Colucci, W.S. “Role of nitric oxide in the regulation of myocardial function.” *Prog. Cardiovasc.* **1995,** *Dis.* 38, 155-166.

5. Bogdan, C.T., Rollinghoff, M. & Diefenbach, A. “The role of nitric oxide in innate immunity.” *Immunological Reviews.* **2000,** 173, 17-26.

6. Karp, Gerald. “The Role of NO as an Intracellular Messenger.” Cell and Molecular Biology. 5th ed. John Wiley & Sons. **2008**, 652-653.

7. Boon, E.M., Marletta, M.A. “Ligand specificity of H-NOX domains: From sGC to bacterial NO sensors.” *Journal of Inorganic Biochemistry*. **2005,** 99, 892-902.

8. Boon, E.M., Davis, J.H., Karow, D.S., Huang, S.H., Tran, R.; Miazgowicz, M.M., Mathies, R., Marletta, M.A. “Characterization of NO binding to prokaryotic homologs of the sGC b1 H-NOX domain.” *Journal of Biological Chemistry*. **2006,** 281, 21892-21902.

9. Boon, E.M., Marletta, M.A. “Ligand discrimination in soluble guanylate cyclase and the H-NOX family of heme sensor proteins.” *Current Opinion in Chemical Biolog.* **2005**, 9, 441-446.

10. Boon, E.M., Huang, S.H., Marletta, M.A. “A molecular basis for NO selectivity in soluble guanylate cyclase.” *Nature Chemical Biology*. **2005,** 1, 53-59.

11. Liu, N., Pak, T., Boon, E.M. “Characterization of a diguanylate cyclase from Shewanella woodyi with cyclase and phosphodiesterase activities” *Molecular Biosystems.* **2010,** 6, 1-4.

12. Lee, V.T. *et al.* “A cyclic-di-GMP receptor required for bacterial exopolysaccharide production.” *Mol. Microbiol.* **2007,** 65, 1474-1484.

13. Hickman, J.W., Tifrea, D.F., Harwood, C.S. “A chemosensory system that regulates biofilm formation through modulation of cyclic diguanylate levels.” *Proc. Natl. Acad. Sci. U. S. A.* **2005**, 102, 14422-14427.

14. Tucker, J.M., Oyola, R., Gai, F. “A Novel Fluorescent Probe for Protein Binding and Folding Studies: *p*-Cyano-Phenylalanine.” *Biopolymers.* **2006,** 83, 571-576.

15. Xue, Y., Xu, Y., Liu, Y., Ma, Y., Zhou, P. “*Thermoanaerobacter tengcogensis* sp. nov., A Novel Anaerobic, Saccharolytic, Thermophilic bacterium Isolated From A Hot Spring in Tengcong, China.” *International Journal of Systematic and Evolutionary Microbiology.* **2001,** 51, 1335-1341.

16. Pellicena, P., Karow, D.S., Boon, E.M., Marletta, M.A., Kuri. “Crystal structure of an oxygen-binding heme domain related to soluble guanylate cyclases.” *Proc.Natl.Acad.Sci.Usa*. **2004,** 101**,** 12854-12859.

17. Olea, C., Boon, E.M., Pellicena, P., Kuriyan, J., Marletta, M.A. “Probing the function of heme distortion in the H-NOX family.” *American Chemical Society Chemical Biology*. **2008**, 3, 703-710.

18. Karp, Gerald. “Fluorescence Microscopy (and Related Fluorescence-Based Techniques).” Cell and Molecular Biology. 5th ed. John Wiley & Sons. **2008**, 731-733.

19. Schmidt, I., Steenbakkers, P.J.M., op den Camp, H.J.M., Schmidt, K., Jetten, M.S.M. "Physiologic and Proteomic Evidence for a Role of Nitric Oxide in Biofilm Formation by Nitrosomonas europaea and Other Ammonia Oxidizers." *Journal of Bacteriology.* **2004,** 186, 9, 2781-2788.

Chapter 2: Progress Towards FRET of *Sw*H-NOX

2.1 Summary

The proposed mechanism for the bacterial nitric oxide signaling pathway is that H-NOX binds NO which subsequently interacts with downstream effectors. Having no enzymatic activity of its own, H-NOX must somehow change its conformation into an active form as to interact with other proteins. In this study, we worked towards understanding the conformational changes in the *Shewanella woodyi* H-NOX protein upon ligand binding using FRET with the unnatural fluorescent amino acid pCN. The FRET pair of pCN and tryptophan was mutated into several positions on wild-type *Sw*H-NOX and the P117A mutant and FRET was performed using a fluorometer. Preliminary data suggests that there was a FRET signal and that there is a difference in distances between pCN and tryptophan in the same respective positions in the wild-type and P117A mutant.

2.2 Introduction

Prokaryotic nitric oxide signaling has been shown to be involved in biofilm formation[1,8]. Studying this pathway can lead to insights on the factors influencing biofilm formation. Biofilms are known to cause infection because of their antibiotic resistance. As a first step in this pathway, nitric oxide is thought to bind H-NOX, which then interacts with DGC, leading to changes in c-di-GMP levels and ultimately biofilm formation. We hypothesize that H-NOX undergoes a conformation change upon ligand binding and subsequently interacts with DGC.

H-NOX binds NO using a heme cofactor. Normally heme cofactors adopt a planar conformation however in H-NOX, the heme is distorted due to the presence of a proline in the heme pocket[2,3]. The crystal structure of the P115A mutant of *Tt*H-NOX reveals that the heme adopts a more planar conformation without the proline. Crystallography has revealed that both ligand binding and proline mutation result in a shift in N-terminal helices. Thus, we hypothesize that the P115A mutant of *Tt*H-NOX mimics the active form of wild-type H-NOX. Therefore in these experiments we plan to compare FRET efficiency in wild-type and P115A structure, as well as wild-type bound to various ligands in order to understand ligand-induced conformational changes in H-NOX. Comparing the differences in distances between pCN and tryptophan using FRET in the wild-type *Sw*H-NOX, the P117A mutant (the homolog to the *Tt*H-NOX P115A mutant) and the NO-bound, wild-type *Sw*H-NOX will confirm that the P117A mutant mimics the NO-bound wild-type.

The experimental design we used involved incorporating the FRET pair of pCN and tryptophan into *Sw*H-NOX in several different locations. *Sw*H-NOX was used in these experiments because it lacks any tryptophan of its own; this meant we could place both the pCN and tryptophan in any location we desired. These locations were determined by comparing the *Tt*H-NOX and the P115A crystal structures and determining which positions in the primary sequence of H-NOX move with respect to each other and would thus be expected to yield changes in FRET efficiency.

Several different positions were chosen for incorporating tryptophan and pCN into *Sw*H-NOX. Positions were chosen based on the largest differences between the wild-type and the P115A, whether we believed it would be a conservative mutation (so that it

would not hinder protein structure), and if the particular residue we replaced was conserved in the H-NOX family. Since the crystal structure of *Tt*H-NOX was used, we used a sequence alignment to determine the corresponding residues on *Sw*H-NOX. Shown in Figure 2-1 are the locations of the computer generated mutations, the distances between the beta-carbons of the residues and the helices where which they reside.

Differences in Distance for Potential Mutations in Wild Type and P115A Tt H-NOX							
	V22W+F152pCn	V22W+L144pCN	W67+F152pCN	W67+L144pCN	V70pCN+F152W	V70pCN+L144W	W67+F82pCN
Wild Type	29-30Å	22-23Å	21-22Å	11-12Å	17-17.5Å	10-11Å	23-24Å
P115A	28-29Å	20-21Å	20-21Å	12-13Å	18-19Å	11-12Å	20-21
Difference	1-2Å	2-3Å	1-2Å	1-2Å	.5-1.5Å	1-2Å	3-4Å
	|---helices B and G----|		|----helices D and G----|		|----helices D and G----|		helix D

Figure 2-1. Distances between residues as determined by PyMOL.

Figure 2-2 below shows the corresponding mutations that were made in the *Sw*H-NOX as determined by the sequence alignment. Two out of the seven *Tt*H-NOX mutations were not used, V70pCN F152W and V22W F152pCN, because we felt that the difference in distances were too miniscule to be detected by FRET.

Mutations in *Sw*H-NOX Corresponding to the Computer Generated *Tt*H-NOX mutations					
***Tt*H-NOX**	V22W L144pCN	W67 L144pCN	V70pCN F152W	V70pCN L144W	W67 F82pCN
***Sw*H-NOX**	L22W L146pCN	V67W L146pCN	F70pCN F154W	F70pCN L146W	V67W H82pCN

Figure 2-2. Corresponding mutations in *Sw*H-NOX as determined by sequence alignment

In addition to all these mutants, a corresponding P117A mutation was made to each double mutant to have a total of 5 double and 5 triple *Sw*H-NOX mutants. All combinations of single mutants with and without P117A were made also for controls (Appendix II). Once we mutated pCN and tryptophan into these positions, purified the proteins, and subjected them to the fluorometer, we expected the FRET data to match the distances determined in Figure 2-1. To support our hypothesis, the FRET distances for the wild-type proteins bound to NO would have to match the predicted distances of the P115A mutants as shown in Figure 2-1. If so, then that means that the NO-bound wild-type protein has a similar conformation as the P115A mutant.

A unique system had to be used to incorporate the unnatural amino acid which involved the vector pDULE2 (Figure 2-3)[4]. pDULE2 codes for a specific aminoacyl-tRNA synthetase that charges pCN onto a tRNA, also coded by this vector, that recognizes the amber codon, UAG. After mutating in the amber and tryptophan codons into *Sw*H-NOX, a certain autoinduction media that promotes the incorporation of pCN was used to grow the cells and express the protein. After purifying the proteins, we could run the FRET experiments using a fluorometer and determine the distances between the donor (pCN) and the acceptor (tryptophan) using the following equations.

$$E = 1 - \frac{\tau'_D}{\tau_D} \qquad E = \frac{1}{1 + (r/Ro)^6}$$

E is the FRET efficiency, τ'_D and τ_D are the donor fluorescence lifetimes in the presence and absence of an acceptor, respectively, *Ro* is the Förster distance, and *r* is the distance between the donor and acceptor[5].

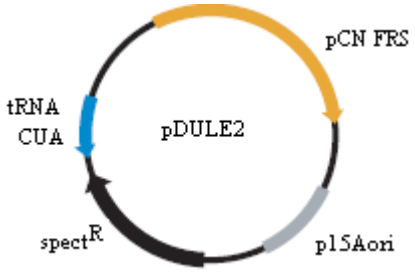

Figure 2-3. pDULE2 vector.

By knowing the active form of H-NOX we can then further hypothesize how it manages to relay its signal to downstream effectors.

2.3 Methods

2.3.1 Determining Sites for pCN and Tryptophan incorporation

The crystal structure of wild-type *Tt*H-NOX and its P115A mutant were used as a model for our experiments. The PyMOL computer program was used to measure distances between certain residues on different helices in both proteins. The same residues were artificially mutated on both the wild-type and P115A and distances were measured between beta-carbons of the 2 residues using the program. Sequence alignments between *Tt*H-NOX and *Sw*H-NOX showed us which resides on *Sw*H-NOX corresponded to the residues on *Tt*H-NOX. The residues that were chosen to be mutated are shown in Figure 2-1. The corresponding *Sw*H-NOX resides are shown in Figure 2-2.

2.3.2 Cloning and Site-Directed Mutagenesis

All of the primers used for cloning and site-directed mutagenesis were purchased from the Stony Brook DNA Sequencing Facility and are shown in the appendix. The *Sw*H-NOX gene was cloned into an invitrogen pBAD/myc-hisC vector using Nco1 and EcoR1 restriction enzymes and other standard New England Biolabs cloning procedures and reagents. The stratagene and phusion protocols and reagents were used to mutate the amber and tryptophan codons into the gene, except for Dpn1 which was from New England Biolabs. All of the mutations made are shown in Figure 2-2 in the *Sw*H-NOX row. All combinations of single mutants with and without P117A were made also for controls (Appendix II). All of the PCR reactions were done in a Bio-Rad thermocycler. After the reactions, the plasmids were chemically transformed into XL1-blue competent cells from strategene. The cells were plated on LB/agar/ampicillin plates and incubated overnight at 37°^{c}. Overnight colonies were inoculated into 3.5ml LB with 10μg/ml ampicillin and incubated for 12-18 hours at 250rpm at 37°^{c}. The plasmids were purified using the Zyppy mini-prep kit. The plasmids from the cloning and site-directed

mutagenesis reactions were sent to the Stony Brook DNA Sequencing Facility for sequencing.

2.3.3 Protein Expression and Purification

The protein expression protocol for pCN incorporation was developed by Dr. Ryan A. Mehl et al. from Franklin and Marshall College[4]. The pBAD.H-NOX plasmids along with pDULE2 were chemically transformed into invitrogens BL21ai cells, plated onto LB/ampicillin/spectinomycin plates and incubated overnight at 37°^{c}. Overnight colonies were inoculated in 6ml LB with 10μg/ml ampicillin and spectinomycin and incubated for 6-12 hours at 250rpm at 37°^{c}. During incubation, the autoinduction media was prepared according to the protein expression protocol. The autoinduction media was inoculated with the growing cells needing no further induction. pCN, purchased from PepTech, was added to the media about 30-60 minutes after inoculation. For wild-type or P115A *Sw*H-NOX with no amber codon, protein expression finished at about 12-14 hours at 250rpm at 37°^{c}. For *Sw*H-NOX expression with the amber codon, expression took 30-32 hours at 250rpm at 37°^{c}. Standard protein purification and quantification procedures done in the Boon lab were used to purify and quantify the protein. The proteins were stored at -80°^{c} in phosphate buffer.

2.3.4 Mass Spectroscopy

In order to confirm successful mutations, the proteins were subjected to MALDI mass spectroscopy. 2μl of trypsin digested peptides were mixed with 8μl of matrix (70/30 acetonitrile/water, 0.1% TFA, and 10mg/ml α-cyano-4-hydroxycinnamic acid). Different matrix:peptide combinations were tried also, including 3:1 and 2:1. Samples were spotted

and dried on a MALDI target plate and were analyzed in the MALDI-TOF provided by the ICB&DD at Stony Brook University.

2.3.5 Fluorescent Assays

All of the proteins in the fluorescent assays were reduced to Fe^{3+} using potassium ferricyanide. The proteins were then quantified with a UV-Vis at about 412nm (Fe^{3+} unligated heme absorption) and diluted in phosphate buffer to about 5μM in a quartz cuvette. Using an Applied Photon Technologies fluorometer from the Raleigh lab, the proteins were scanned from 260nm to 350nm at a slit width of 1.2mm.

2.4 Results and Discussion

Incorporating pCN using the amber codon into *Sw*H-NOX proved to be extremely variable and unpredictable. Identical expression methods were used for each *Sw*H-NOX variant; some variants expressed flawlessly while others did not express at all. To illustrate this, Figures 2-4 and 2-5 show examples of coomassie stained protein gels of particular protein purifications of L146pCN and L146pCN L22W P117A, respectively. The gels show protein fractions collected after eluting from a nickel affinity column.

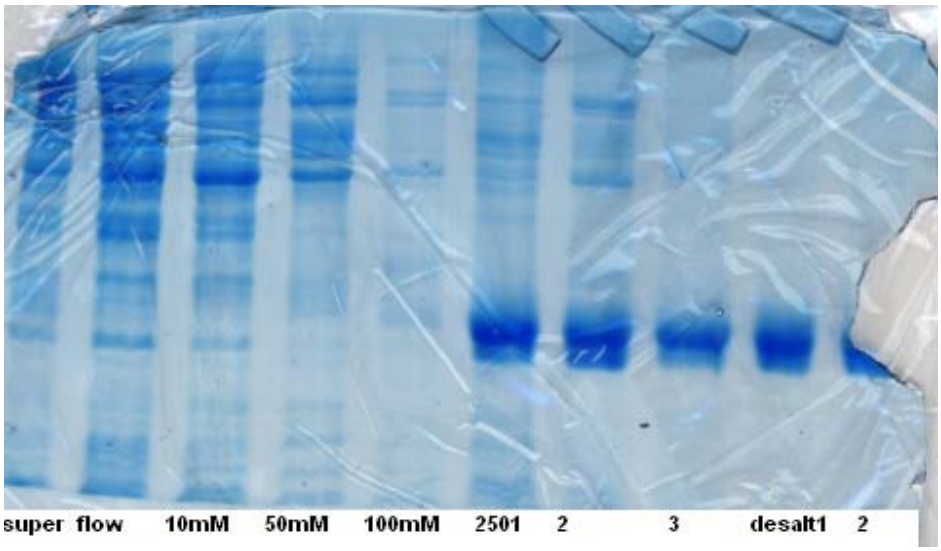

Figure 2-4. Purification of L146pCN using nickel affinity chromatography and increasing concentrations of imidizole. Several fractions of protein were collected and shown on the right

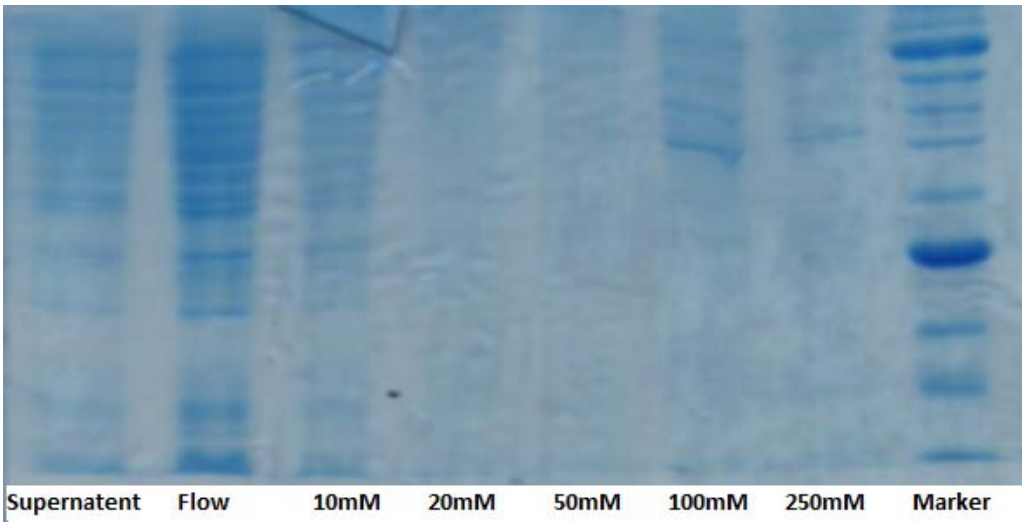

Figure 2-5. Purification of L146pCN L22W P117A using nickel affinity chromatography and increasing concentrations of imidizole.

The protein purification in Figure 2-4 shows a significant amount of pure protein in the gel after it came off the nickel column while Figure 2-5 shows little to no detectable protein. One hypothesis attributed this variability to mRNA hairpins near the ribosomal binding site that reduced expression to the already inefficient protein synthesis[6]. Using an online mRNA hairpin energy calculator, we reduced the supposed mRNA hairpin on our F70pCN mutant using site-directed mutagenesis. The expression remained low to none. The reason why expression did not work with all the mutants and why some worked better than others remains unknown.

The position that seemed to work was the L146pCN position which proved to have the best protein expression out of all the other mutants. Several single, double and triple mutants were expressed, purified and scanned using the fluorometer; these included L146pCN, L146pCN L22W, L146pCN V67W, and L146pCN V67W P115A. The L146pCN V67W P115A expressed poorly and the L146pCN L22W P115A did not express at all. We attempted to confirm these mutations using MALDI mass

spectroscopy, however several desired peaks were not seen on the spectra, as seen in Figures 2-6 to 2-10.

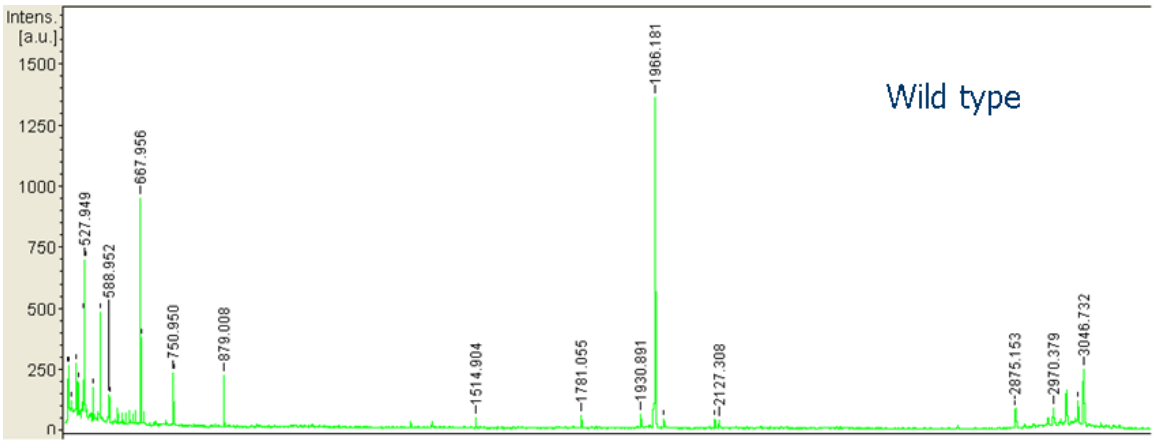

Figure 2-6. Wild-type *Sw*H-NOX MALDI spectrum.

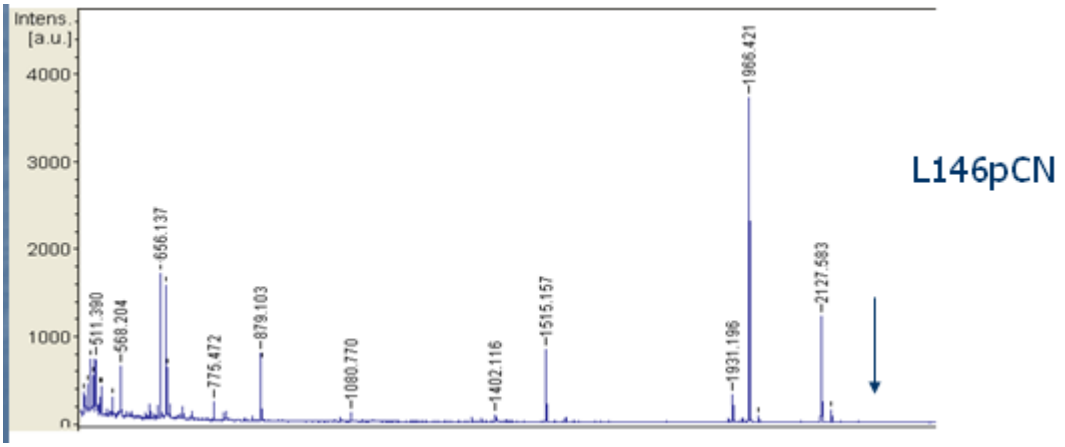

Figure 2-7. L146pCn *Sw*H-NOX MALDI spectrum.

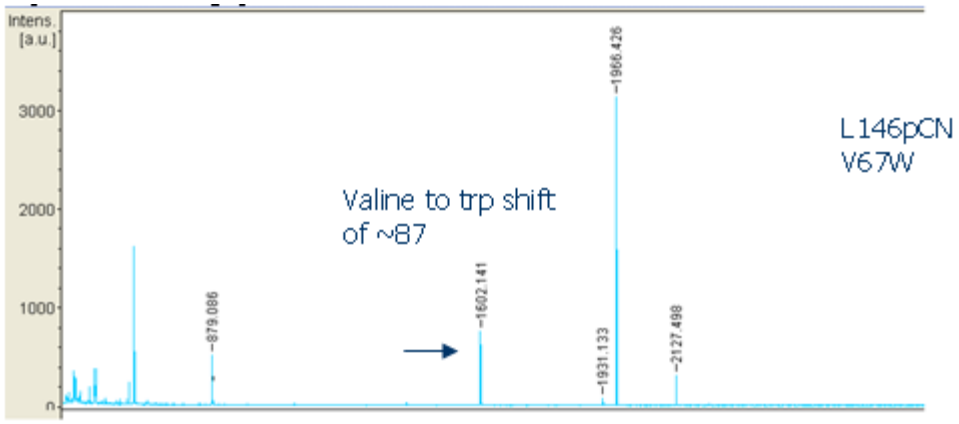

Figure 2-8. L146pCN V67W *Sw*H-NOX MALDI spectrum.

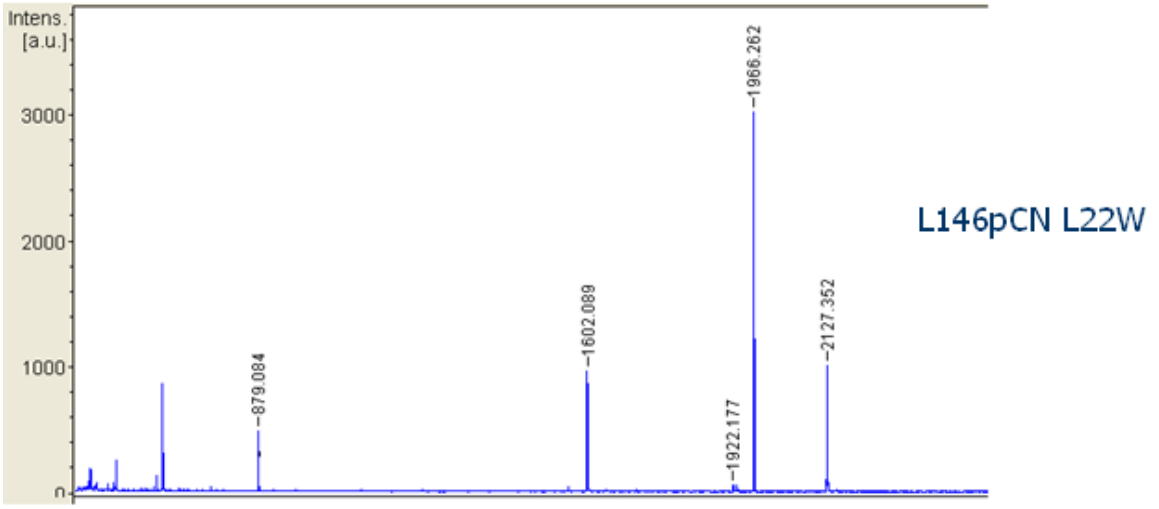

Figure 2-9. L146pCN L22W *Sw*H-NOX MALDI spectrum.

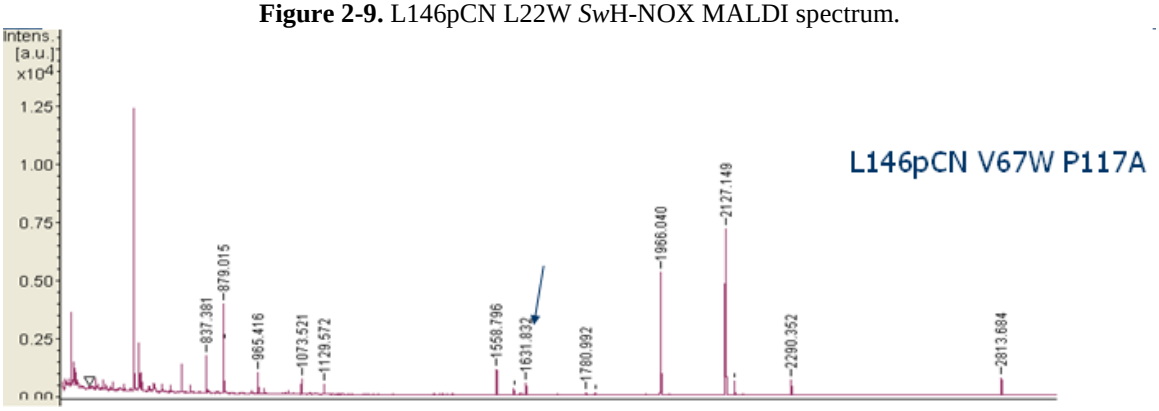

Figure 2-10. L146pCN V67W P117A *Sw*H-NOX MALDI spectrum.

Figure 2-6 shows the wild-type *Sw*H-NOX MALDI spectrum; L146 should be in a peak around 2122m/z, however this peak is not seen in this spectrum. In addition, the expected shift from 2122m/z to 2181m/z, L46pCN, was not seen in Figure 2-7 (as indicated by the arrow) or any of the following spectra. This was significant because all of these proteins should have had this peak shift but it was not seen in any spectra. This could be because perhaps that particular peptide did not travel as well as the others. In Figure 2-8, a shift from 1514m/z to 1602m/z indicates that a V67W mutation is present. In Figure 2-9, the peptide that contains L22 was too large to fly or be seen on MALDI; a full protein mass spectroscopy spectrum would be able to detect the L22W mutation. The L146pCN V67W P117A, Figure 2-10, protein did not express well, so there were several

missed cleavages because of low concentration of protein; if we take into account a particular missed cleavage at K120, the expected 1680m/z to 1631m/z peak shift may correspond to a P117A mutation.

To perform the FRET, fluorescent assays were done using the fluorometer and are shown below in Figures 2-11 and 2-12. In the spectra, the proteins were excited at 240nm, which is the approximate absorptive maximum for pCN, and emission wavelengths were detected between 260nm and 350nm to detect tryptophan emission that ranges from 300nm to 350nm, depending on its surrounding environment[9].

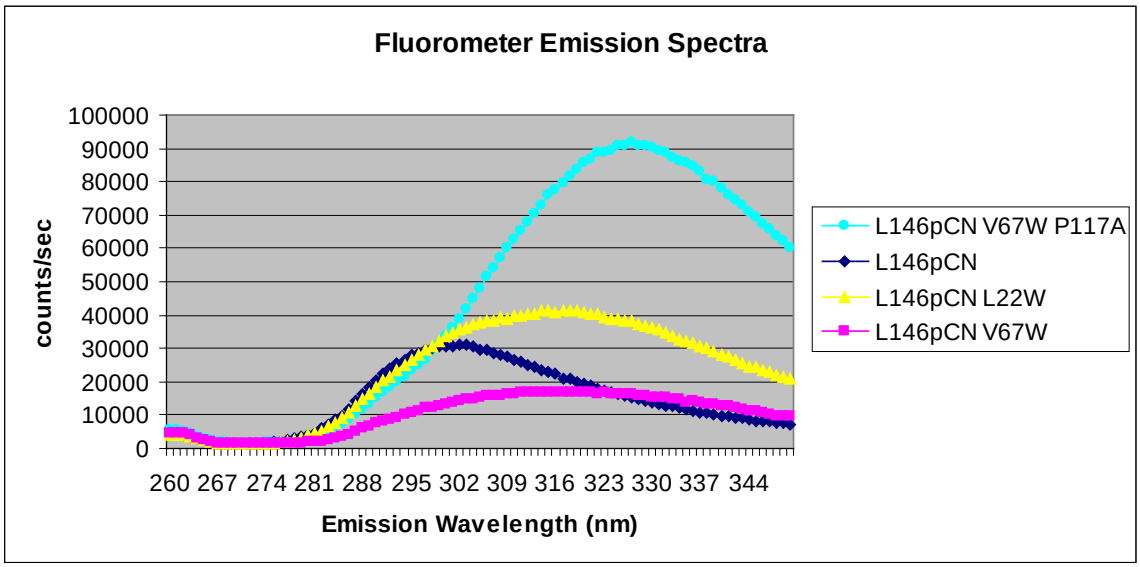

Figure 2-11. Emission spectra of several *Sw*H-NOX variants.

The spectrum that shows L146pCN alone has a maximum value at 302nm. This is close to the expected value of 290nm because that is the emission maximum of pCN when it is alone in solution[9]. It can be seen that the addition of a tryptophan changes the emission spectra of the protein when compared to the L146pCN alone. The emission maximum for L146pCN V67W P117A, L46pCN L22W and L146pCN V67W were 329nm, 318nm, and 313nm, respectively. As stated earlier, the emission of tryptophan is between 300nm and 350nm so these values were accepted. According to the FRET

equations, τ'_D equals the lifetime of the donor without the acceptor (L146pCN alone) and τ_D equals the lifetime of the donor and acceptor at that same wavelength. For example, τ'_D equals 31004.6 which occurs at 302nm for L146pCN. At that same wavelength, τ_D equals 35887.5 for L146pCN L22W, 14219.3 for L146pCN V67W, and 38792.8 for L16pCN V67W P117A. The only spectrum that can be used for the equations would be L146pCN V67W; L146pCN L22W and L16pCN V67W P117A would result in negative values for *E* which means we would be unable to find the distance between the donor and acceptor using the second equation when solving for *r*. The equations for L146pCN V67W are solved below.

L146pCN V67W

$E = 1-(14219.3/31004.6) = 0.541$

$0.541 = 1/(1+(r/16)^6)$

$r = 15.57$Å

According to the equations, the distance between L146pCN and V67W is 15.57Å. The predicted distance between L144pCN and W67 (residues that corresponded with *Sw*H-NOX L146pCN and V67W) was 12-13Å on the *Tt*H-NOX model according to the PyMOL computer program. This is a difference of about 2-3Å from the predicted to the measured values.

Another fluorescent spectra was run, however this time the L146pCN V67W P117A was omitted because it would not seem to express as well as it did before after several attempts.

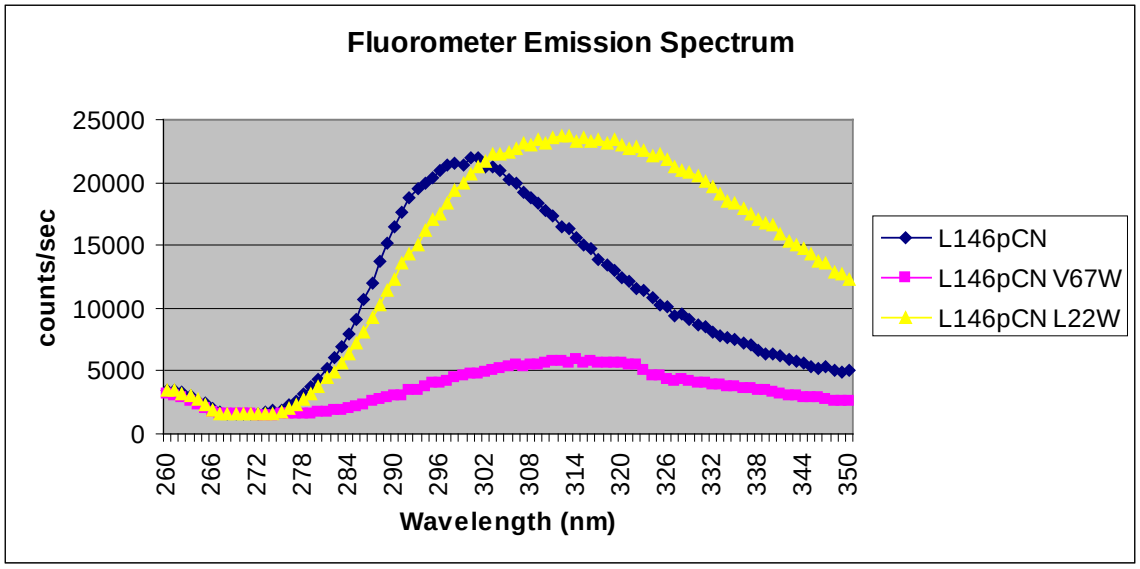

Figure 2-12. Emission spectra of several *Sw*H-NOX variants without L146pCN V67W P117A.

Similar wavelength emission maxima were seen on this spectra as was seen in Figure 2-11. According to this spectra, τ'_D equals 22081.4 which occurs at 300nm for L146pCN. At that same wavelength, τ_D equals 4808.11 for L146pCn V67W and 20604.6 for L146pCn L22W. The equations for L146pCn V67W and L146pCn L22W are solved below.

L146pCN V67W

$E = 1-(4808.1/22081.4) = 0.782$

$0.782 = 1/(1+(r/16)^6)$

$r = 12.93$Å

L146pCN L22W

$E = 1-(20604.6/22081.4) = 0.0669$

$0.0669 = 1/(1+(r/16)^6)$

$r = 24.83$Å

According to the equations, the distance between L146pCN and V67W is 12.93Å. Again, the predicted distance between L144pCN and W67 was 12-13Å on the *Tt*H-NOX model. The predicted and measured values in this spectra matched. The measured distance between L146pCN and L22W is 24.83Å. The predicted distance between

L144pCN and V22W (residues that corresponded with *Sw*H-NOX L146pCN and L22W) was 22-23Å on the *Tt*H-NOX model according to PyMOL. This is a difference of about 1Å from the predicted to the measured values.

It is not clear why the spectra shown in Figure 2-11 resulted in some unusable data and data that did not match our predicted values, perhaps it was a user error because it was our first experiment using the machine, but the repeated fluorescent assay (Figure 2-12) resulted in distances that were close to the predicted values. Preliminary interpretations of these results can be that the *Tt*H-NOX crystal structure proved to correspond well to the *Sw*H-NOX protein since the measured distances were close to the predicted distances. In other words, we could use PyMOL and the *Tt*H-NOX crystal structure to accurately predict distances between residues in *Sw*H-NOX. Of course, we can not make any other predictions in *Sw*H-NOX structure unless other fluorescent experiments are done on other mutants with and without NO bound and the P117A mutation. However, these results do seem promising and we possibly would be able to determine whether the P117A mutant mimics the NO-bound wild-type using these types of experiments.

Preliminary data shows that the use of pCN and tryptophan as a FRET pair could be useful in determining the intramolecular distances between them and, in turn, could infer how a protein changes its shape. Further studies need to be done with and without NO bound to these proteins along with the appropriate P117A mutants. It proved very difficult to express these proteins because of the inefficient, unpredictable, and largely unknown mechanism of unnatural amino acid incorporation. These experiments can become streamlined once an efficient and reliable procedure is created to incorporate

pCN into *Sw*H-NOX. If and when that happens, we will be able to determine the changes in *Sw*H-NOX structure using pCN and FRET.

2.5 References

1. Liu, N., Pak, T., Boon, E.M. "Characterization of a diguanylate cyclase from Shewanella woodyi with cyclase and phosphodiesterase activities" *Molecular Biosystems.* **2010,** 6, 1-4.

2. Pellicena, P., Karow, D.S., Boon, E.M., Marletta, M.A., Kuri. "Crystal structure of an oxygen-binding heme domain related to soluble guanylate cyclases." *Proc.Natl.Acad.Sci.Usa*. **2004,** 101**,** 12854-12859.

3. Olea, C., Boon, E.M., Pellicena, P., Kuriyan, J., Marletta, M.A. "Probing the function of heme distortion in the H-NOX family." *American Chemical Society Chemical Biology.* **2008**, 3, 703-710.

4. Hammill, J.T., Miyake-stoner, S., Hazen, J.L., Jackson, J.C., Mehl, R. "Preparation of Site-Specifically Labeled Fluorinated Proteins for ^{19}F-NMR Structural Characterization." *Nature Protocols.* **2007**, 2, 10, 2601-2607.

5. *FRET*. Wikipedia, 26 Nov. 2010. Web. 28 Nov. **2010**. <http://en.wikipedia.org/wiki/F%C3%B6rster_resonance_energy_transfer>.

6. Kudla, G., Murray, A.W., Tollervey, D., Plotkin, J.B. "Coding-Sequence Determinants of Gene Expression in *Escherichia coli.*" *Science.* **2009**, 324, 255-258.

7. The PyMOL Molecular Graphics System, Version 1.3r3pre, Schrödinger, LLC.

8. Schmidt, I., Steenbakkers, P.J.M., op den Camp, H.J.M., Schmidt, K., Jetten, M.S.M. "Physiologic and Proteomic Evidence for a Role of Nitric Oxide in Biofilm Formation by Nitrosomonas europaea and Other Ammonia Oxidizers." *Journal of Bacteriology.* **2004,** 186, 9, 2781-2788.

9. Tucker, J.M., Oyola, R., Gai, F. "A Novel Fluorescent Probe for Protein Binding and Folding Studies: *p*-Cyano-Phenylalanine." *Biopolymers.* **2006,** 83, 571-576.

Chapter 3: Determining the Conformational Changes of *Tt*H-NOX using Computational Simulations

3.1 Summary

Throughout the years, computational simulations have been proven to replicate laboratory experimental data, whether it be molecular motion, drug binding energies, etc. Given crystal structure or NMR coordinates of a protein, computational force field programs could potentially predict the motions of the protein in a given time scale, giving insight on how the protein functions. The crystal structure of *Tt*H-NOX and its P115A mutant have been solved and will be used in these computational experiments. The active, NO bound, form of *Tt*H-NOX is thought to be mimicked by the P115A mutant. By running computational simulations of *Tt*H-NOX with and without NO bound, we may be able to observe it converge into the P115A conformation when NO is bound.

3.2 Introduction

The H-NOX family of proteins are predicted to be involved in signal transduction pathways where small gas molecules bind the heme and elicit a conformational change. Interestingly, these proteins all contain extremely distorted heme groups due to the presence of a proline in the heme pocket[1,2]. This observation has led to the hypothesis that flattening of the heme is coupled with ligand binding and, therefore, activation of the protein through a conformational change.

Computational simulation is a very powerful tool as it can reproduce laboratory experiments and enlighten us on protein motion. Conformational changes in proteins are extremely important to understand because it is these changes that allow proteins to perform certain acts, whether its catalysis, protein-protein interactions, facilitated diffusion, etc. Our purposes require us to build protein, heme and gas models of *Tt*H-

NOX and its P115A mutant and simulate how it changes upon NO binding. To help assess conformational changes in the protein and heme, root mean square deviation (RMSD) values of the amino acid backbone, certain helices and dihedral angels of the heme will be measured on the restrained and unrestrained simulations using ptraj. Large RMSD values can be interpreted as significant changes from the original crystal structure as the simulation tries to minimize the energy of the system. We hypothesize that oxygen bound to *Tt*H-NOX (the original crustal structure) is going to have minimal changes in RMSD because it already is in its lowest energy conformation. However, once NO binds, H-NOX and the heme should change its shape and deviate from the original, oxygen bound, crystal structure. The P115A mutant should not have large RMSD values in either the oxygen or NO bound simulations because, again, it is a model for active *Tt*H-NOX.

In *Tt*H-NOX, the heme center iron is coordinated with an axial histidine 102. Displacement of this histidine causes a shift in helix F (Figure 1-6) that reshapes the heme and protein into similar positions as the P115A mutant[3]. NO would be capable of coordinating with the iron and displacing the histidine to cause this change in shape as illustrated by Figure 3-1.

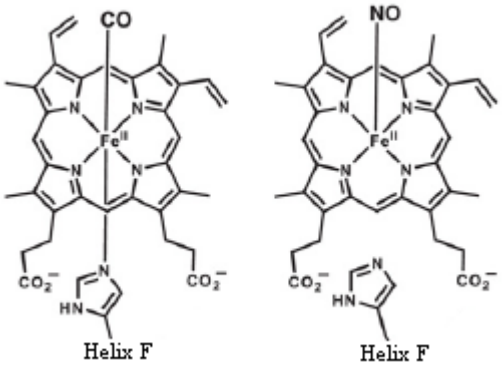

Figure 3-1. NO displaces the axial histidine while carbon monoxide or oxygen would be unable to[3].

It is important to note that some H-NOX proteins do not have the capability to bind oxygen, carbon monoxide or other gases, which is additional evidence that NO is the only gas that would be able to elicit a response.

Because of its significance, it would be interesting to study and observe the conformational change of *Tt*H-NOX upon the binding of NO through computational simulations. In addition, computational simulations may reveal that the NO bound form of *Tt*H-NOX is similar, if not identical, to the P115A mutant. Studying these changes is important to elucidate how H-NOX contributes to biofilm formation.

3.3 Methods

3.3.1 PDB File Setup

The crystal structure of oxygen bound *Tt*H-NOX has been solved and was used as the starting structure (PDB code: 1U4H). Since oxygen does not elicit a response and does not displace the axial histidine, it is acceptable to compare the oxygen bound structure to the unligated structure. Using USCF Chimera[6], this structure was stripped down to its essential components, the heme, protein and gas, each having its own PDB file. In addition, oxygen was switched to NO using chimera; the PDB of NO gas was also saved. Similar methods were used on the oxygen bound P115A mutant (PDB code: 3EEE) to generate separate PDB files for the heme, protein and gas.

3.3.2 AMBER10 Force Field

Tleap and Antechamber

Tleap and antechamber are AMBER10[7] tools that can prepare files for simulation. Parameters for the heme, prep and frcmod files, were obtained on the AMBER MD website and were created from hemoglobin and myoglobin hemes[4]. Parm and frcmod

files for the gas molecules were generated using antechamber. Using tleap and online tutorials[5], the protein and the heme were combined to create parm and crd files. These files were visualized on VMD[8] to see if they were properly shaped and configured. Again tleap was used but this time it was used to combine the protein, heme and gas, both oxygen and NO, into parm and crd files. VMD was used to visualize these files to see if everything was in order. The leaprc.ffSB[9] force field was used for the protein and leaprc.gaff was used for the heme and gas.

Sander

Once these files were created, molecular dynamic (MD) simulations were ready to proceed using Sander, the MD arm of AMBER10 which simulates movement. Constructing the sander scripts for oxygen and NO bound H-NOX complexes were followed from the AMS536 website[5]. The system was solvated in an orthorhombic box of pre-equilibrated TIP3P water 10Å around the protein. These simulations were run with 9 minimization steps and 2 production steps. Amino acid backbone restraints were placed and 2ns of movement were simulated. Parallel simulations were run with backbone restraints during the minimization runs, but were taken away during the 2ns production runs. Similar protocols were used to simulate the P115A mutant with both oxygen and NO bound.

ptraj

Ptraj is an AMBER analysis program that can extract data from our simulations. Using ptraj, RMSD values of the amino acid backbone, certain amino acid residues, dihedral angels, etc can be calculated for each picosecond of simulation. Scripts for ptraj were obtained from the AMBER10 manual. First, water molecules were stripped from the

two production runs and the simulations were condensed into one, striped, 2ns trajectory. Then ptraj was specified to calculate RMSD values of the Cα of given residues. RMSD values were saved as text files and were plotted using Microsoft Excel.

3.3 Results and Discussion

RMSD values from the sander simulations were obtained from ptraj. Figure 3-2 shows the RMSD values of the backbone alpha carbons of both the oxygen and NO bound H-NOX simulations.

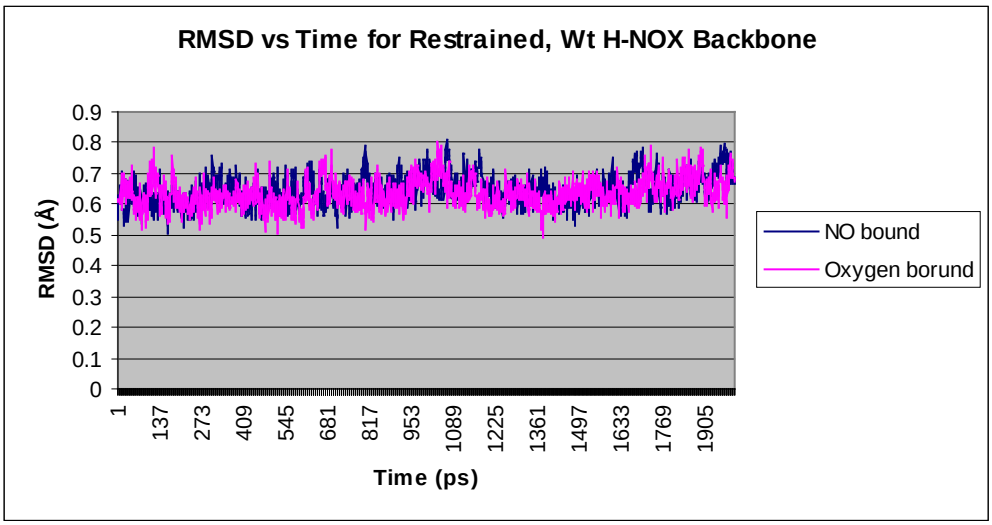

Figure 3-2. RMSD vs Time data for the restrained, wild-type H-NOX backbone with oxygen and NO bound

RMSD values for the backbone carbons in both restrained simulations with oxygen and NO bound seem very stable. Average RMSD values for the oxygen and NO bound structures were 0.645Å and 0.634Å, respectively. Similar results were obtained with backbone restrained P115A simulations (not shown). Average RMSD values for the oxygen and NO bound structures for the P115A mutant were 0.715Å and 0.743Å, respectively. These results were expected because the backbones were restrained and not meant to deviate significantly from the starting crystal structure.

RMSD values of the unrestrained backbone simulations of the wild-type H-NOX with oxygen and NO bound are shown in Figure 3-3.

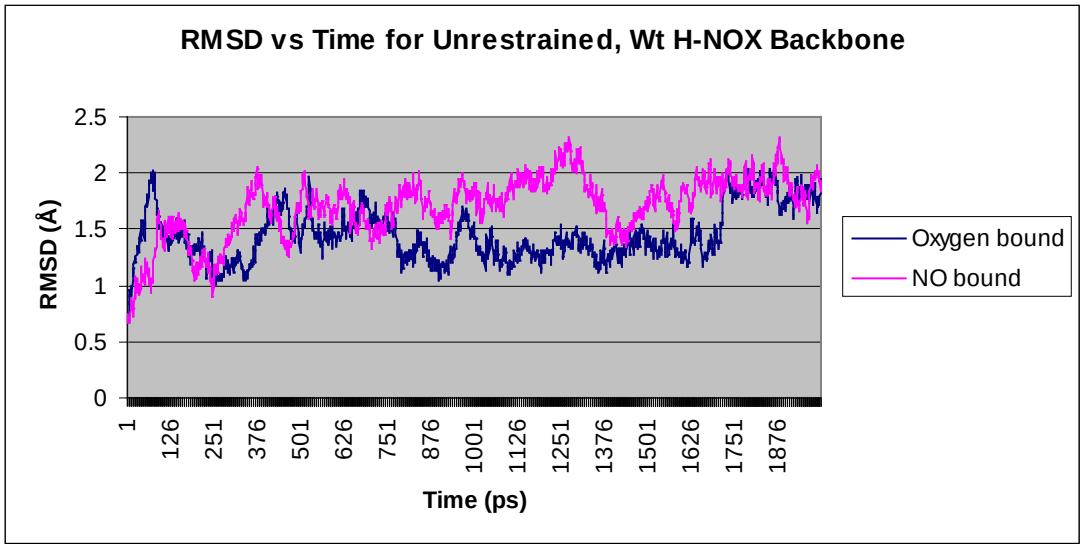

Figure 3-3. RMSD vs Time data for the unrestrained, wild-type H-NOX backbone with oxygen and NO bound

RMSD values for both simulations seem sporadic with the NO bound plot more unstable, but seem to converge after 1.6-1.7ns. Longer simulations would have to be run to confirm whether this is an energetically favorable structure or it is just coincidence that the structures converged at 2ns. Also, it cannot be concluded whether the gas molecule bound to the heme is having an impact on protein structure from this plot. We expected that the NO bound structure would deviate more from the crystal structure than the oxygen bound because NO binding elicits a conformational change in the protein. This plot is inconclusive in showing a stable difference in the two structures; longer simulations would have to be run to confirm whether the structures actually do deviate from one another.

A similar sporadic pattern was observed for the P115A mutant simulations (Figure 3-4). It was predicted that the RMSD for the unrestrained, oxygen or NO bound, P115A simulations would not deviate much from the crystal structure because the P115A

mutant is supposed to mimic the NO bound, wild-type structure. Therefore changing oxygen to NO in the P115A mutant should not change the structure. Again, this simulation needs to be run longer because it is inconclusive whether or not NO binding changes the structure.

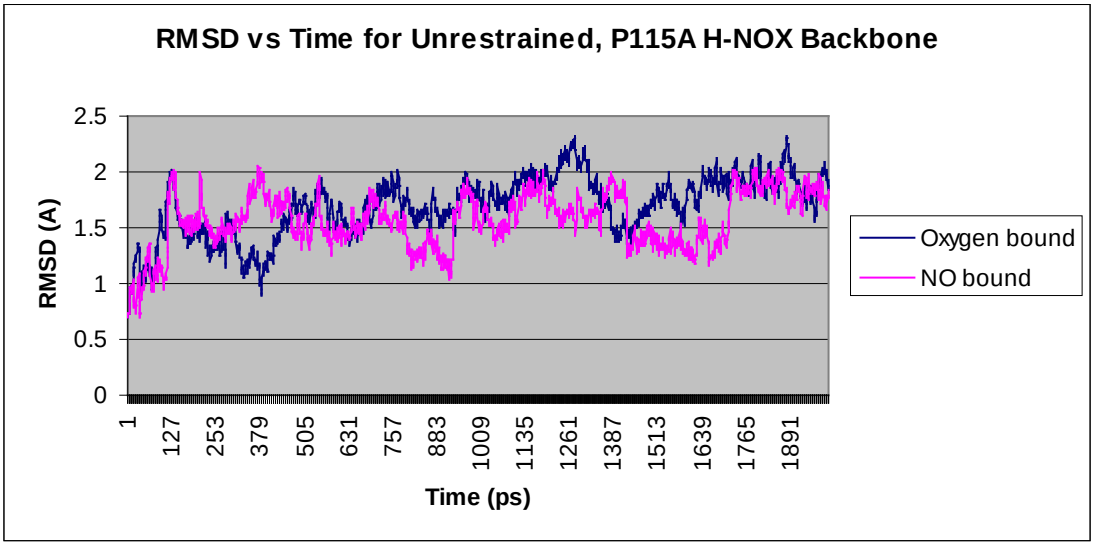

Figure 3-4. RMSD vs Time data for the unrestrained, P115A H-NOX backbone with oxygen and NO bound

For a more specific view on protein structural changes, we can plot Cα RMSD values for a specific helix that it thought to shift when NO binds. Based on the crystal structure of the P115A mutant, helix B (Figure 1-6) moves significantly from its wild-type starting position. Helix B consists of amino acid residues 18-30. A ptraj script was written that specifically probes the RMSD of these residues. Figure 3-5 and 3-6 shows RMSD vs time of helix B of the unrestrained, wild-type H-NOX and unrestrained P115A H-NOX, respectively.

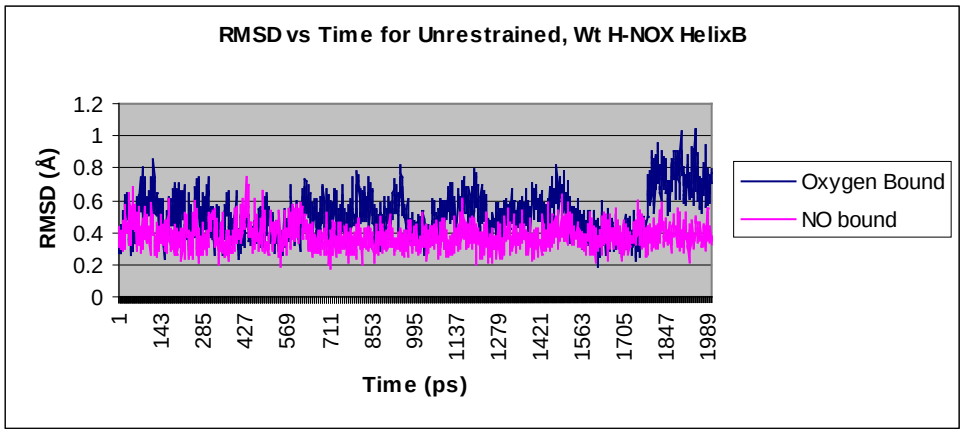

Figure 3-5. RMSD vs Time data for the unrestrained, wild-type H-NOX helixB with oxygen and NO bound

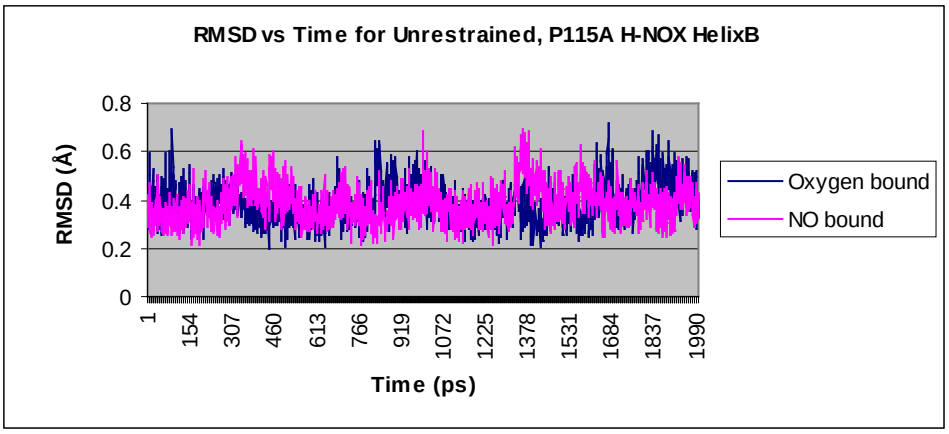

Figure 3-6. RMSD vs Time data for the unrestrained, P115A H-NOX helixB with oxygen and NO bound

These results are more conclusive that the protein is not changing its conformation during the 2ns simulation. The crystal structure of the wild-type H-NOX compared to the P115A mutant does not show a significant change in helix B. A change should have been observed in the wild-type, NO bound plot because NO is supposed to elicit a change in the protein that is similar to the P115A mutant structure. It seems that the RMSD of helix B remains within 0.2 and 0.6Å in all the plots. Unexpectedly, the wild-type, oxygen bound plot in jumps to about 0.8-1.0Å after 1.8ns. Again, the simulation has to be run longer to see if it actually stabilizes at this point or if it is a random fluctuation.

As mentioned earlier, NO is supposed to displace the axial histidine 102 that is coordinated with the heme-bound iron. RMSD values of this particular residue can be obtained from both the wild-type and P115A simulations, Figures 3-7 and 3-8.

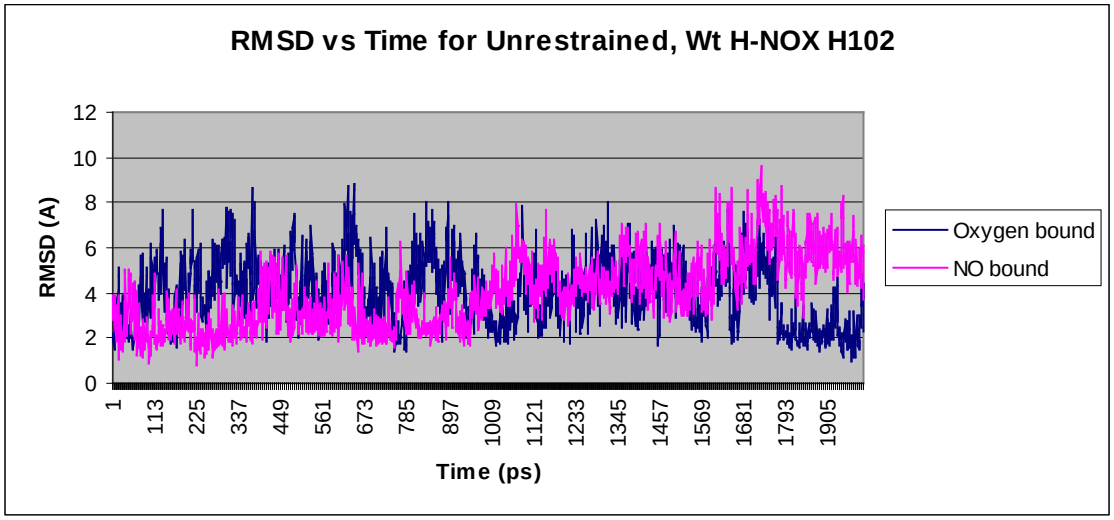

Figure 3-7. RMSD vs Time data for the unrestrained, wild-type H-NOX H102 with oxygen and NO bound

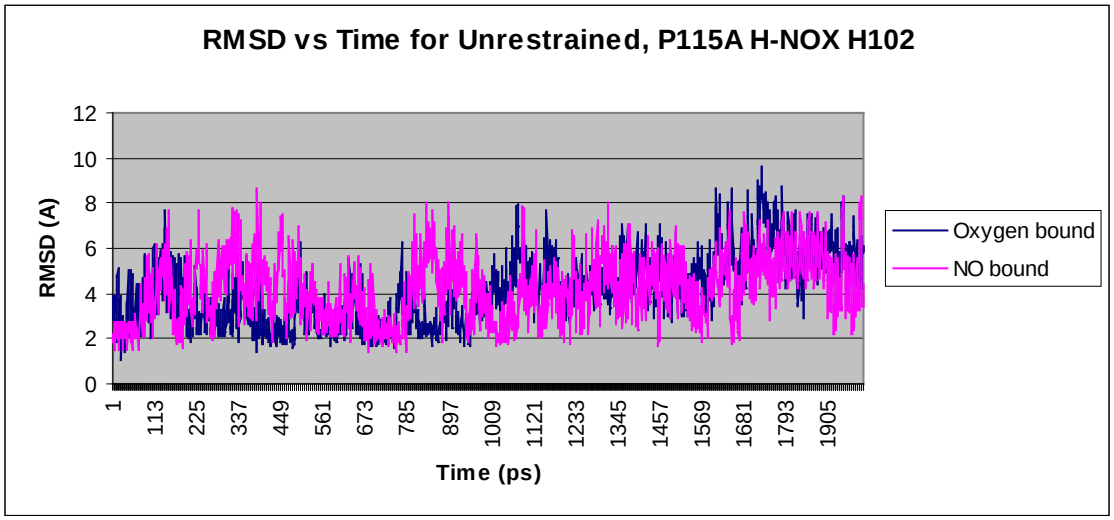

Figure 3-8. RMSD vs Time data for the unrestrained, P115A H-NOX H102 with oxygen and NO bound

H102 is supposed to shift from its original position in the unrestrained, wild-type, NO bound structure. It can be seen in Figure 3-7 that this is not the case. H102 does not remain stable, the RMSD values are very large, but they deviate about the same in the

wild-type and the P115A. Thus, it can be inferred from these simulations that NO is not displacing H102 nor having an effect on protein structure on these time scales.

NO binding, however, should have an effect on heme structure. It is predicted that the distortion of the heme is relaxed once NO binds to the iron because proline 115 is shifted. The heme should assume a flat shape as in the P115A mutant (Figures 1-7 and 1-9). A ptraj script was written that calculated the RMSD of the distorted dihedral angle of the heme between 4 atoms: C2A, CAA, CBA, and CGA. RMSD values of the dihedral angle of the distorted bond were obtained and plotted for wild-type and P115A in Figures 3-9 and 3-10, respectively.

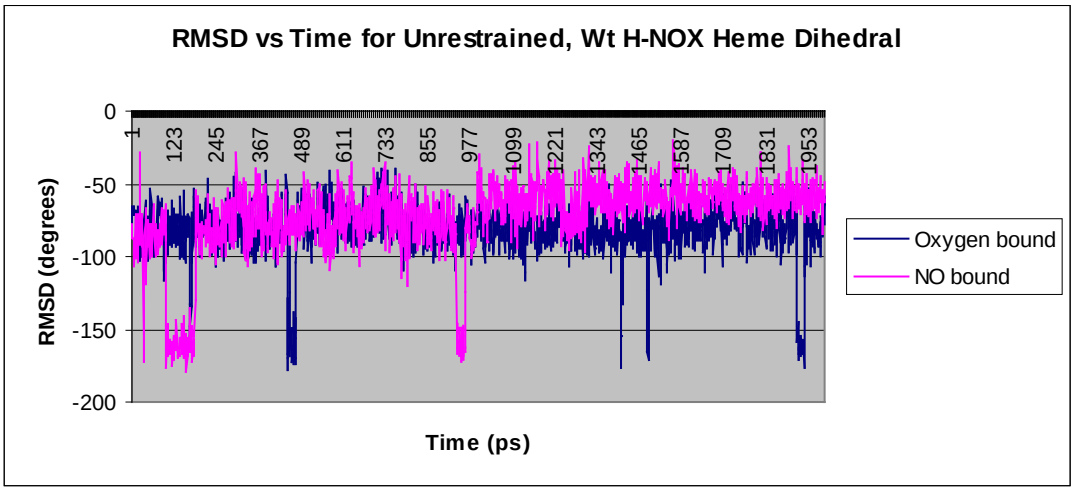

Figure 3-9. RMSD vs Time data for the unrestrained, wild-type H-NOX heme dihedral with oxygen and NO bound

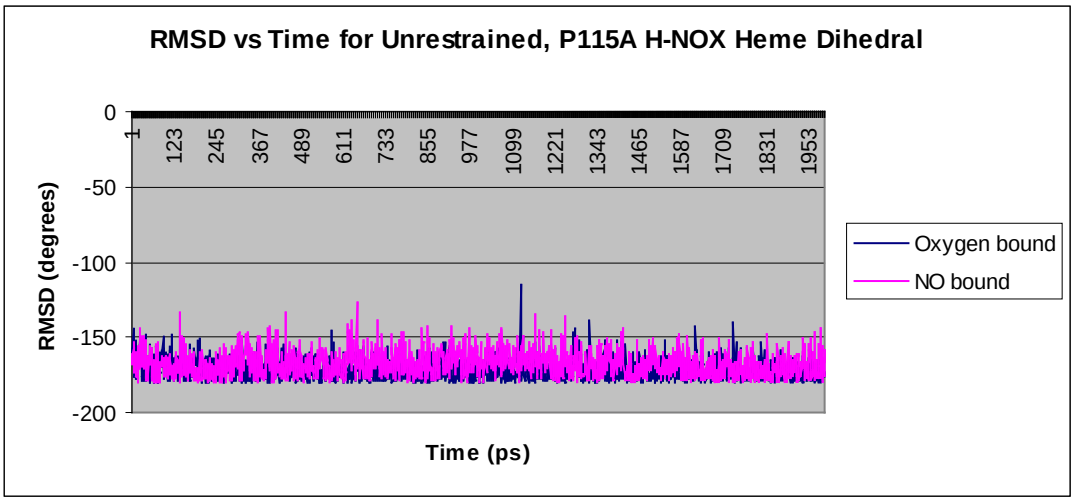

Figure 3-10. RMSD vs Time data for the unrestrained, P115A H-NOX heme dihedral with oxygen and NO bound

The NO bound heme should have converged towards a flatter, -180º angle similar to the P115A mutant heme. Although it did not converge, the flatter conformation was sampled at several time points in both wild-type plots.

It is clear through these plots that NO is not having an effect on heme or protein structure. The unrestrained backbone, helix B, H102 and heme dihedral plots show no significant difference between the oxygen and the NO bound structures. The first step towards a conformation change would be the displacement of H102 and a subsequent flattening of the heme. The H102 plot and heme dihedral plot show that there is little to no deviation from the original, oxygen bound, crystal structure. This leads towards the conclusion that NO is not having the predicted effect of flattening the heme and changing the conformation of the protein on these time scales.

This study attempted to simulate the change in conformation between the wild-type, oxygen bound and NO bound proteins. The P115A mutant was used as a positive control because the NO bound wild-type should adapt the same structure as the P115A mutant. However, the analysis of these simulations showed that the NO bound heme-

protein did not change relative to the oxygen bound heme-protein, which was supposed to remain constant. Figure 3-5 shows that a particular helix that was expected to shift did not deviate from its original position. Figure 3-7 shows that H102, which was expected to be displaced, also did not shift. Although it was expected to converge to a flatter conformation, the heme remained distorted and did not flatten out, as shown in Figure 3-9. The flat conformation was sampled several times with NO and oxygen bound, but again, it did not converge to that conformation. This may be attributed to the fact that, in reality, NO binding to iron changes the coordination state of the metal. When NO binds iron, the axial histidine102 is released from the iron through some quantum mechanical mechanism. The charge and quantum mechanical properties on the nitrogen in NO induces this change while other diatomic gases, such as oxygen or carbon monoxide, do not induce this change. The AMBER10 force field may have been able to simulate this complex, transition metal, coordinate chemistry which maybe why the simulations did not behave as they were predicted. There are force fields that specialize in quantum mechanics, such as AMBER QM. This particular project would have been best suited for those advanced types of force fields and any future work should be wary of these properties.

H-NOX proteins are predicted to be an important sensor for NO and are hypothesized to be involved in the biofilm formation pathways. Biofilms have a huge human and ecological impact because of their adhesive, infectious and antibiotic resistant nature. Understanding this pathway is critical if humans are to combat antibiotic resistant biofilms. A first step in this pathway is NO binding to H-NOX, which elicits some kind

of conformational change. This change allows H-NOX to bind to downstream effectors which eventually leads to biofilm formation.

3.5 References

1. Pellicena, P., Karow, D.S., Boon, E.M., Marletta, M.A., Kuri. "Crystal structure of an oxygen-binding heme domain related to soluble guanylate cyclases." *Proc.Natl.Acad.Sci.Usa*. **2004,** 101**,** 12854-12859.

2. Olea, C., Boon, E.M., Pellicena, P., Kuriyan, J., Marletta, M.A. "Probing the function of heme distortion in the H-NOX family." *American Chemical Society Chemical Biology*. **2008**, 3, 703-710.

3. Erbil, W.K., Prince, M.S., Wemmer, D.E., Marletta, M.A. "A structural basis for H-NOX signaling in Shewanella oneidensis by trapping a histidine kinase inhibitory conformation" *PNAS.* **2009,** 16, 47, 19753–19760.

4. Giammona, D.A. **Ph.D. thesis, University of California, Davis (1984)**

5. "2010 AMBER Tutorial with Biotin and Streptavidin" Rizzo, R. 5 May. **2010**. Stony Brook University AMS536. <http://ringo.ams.sunysb.edu/index.php/2010_AMBER _ Tutorial_with_Biotin_and_Streptavidin>

6. Pettersen, E.F., Goddard, T.D., Huang, C.C., Couch, G.S., Greenblatt, D.M., Meng, E.C., Ferrin, T.E. "UCSF Chimera--a visualization system for exploratory research and analysis." *J Comput Chem.* **2004**, 13,1605-12.

7. D.A. Case, T.A. Darden, T.E. Cheatham, III, C.L. Simmerling, J. Wang, R.E. Duke, R. Luo, M. Crowley, R.C.Walker,W. Zhang, K.M. Merz, B.Wang, S. Hayik, A. Roitberg, G. Seabra, I. Kolossvy, K.F.Wong, F. Paesani, J. Vanicek, X.Wu, S.R. Brozell, T. Steinbrecher, H. Gohlke, L. Yang, C. Tan, J. Mongan, V. Hornak, G. Cui, D.H. Mathews, M.G. Seetin, C. Sagui, V. Babin, and P.A. Kollman (2008), AMBER 10, University of California, San Francisco.

8. Humphrey, W., Dalke, A. and Schulten, K., "VMD - Visual Molecular Dynamics." *J. Molec. Graphics*, **1996**, 14, 33-38.

9. Hornak, V., Abel, R., Okur, A., Strockbine, B., Simmerling, C. “Comparison of multiple Amber force fields and development of improved protein backbone parameters.” *Proteins*. **2006**, 65, 3, 712-725.

References

1. Koshlan, D.E. “The Molecule of the Year” *Science.* **1992,** 258, 5090, 1861.

2. Culotta, E., Koshlan, D.E. “NO news is Good News” *Science.* **1992,** 258, 5090, 1862-1865.

3. Toda, N., Okamura, T. “The pharmacology of nitric oxide in the peripheral nervous system of blood vessels.” *Pharmacol.* **2003,** *Rev.* 55, 271-324.

4. Hare, J.M., Colucci, W.S. “Role of nitric oxide in the regulation of myocardial function.” *Prog. Cardiovasc.* **1995,** *Dis.* 38, 155-166.

5. Bogdan, C.T., Rollinghoff, M. & Diefenbach, A. “The role of nitric oxide in innate immunity.” *Immunological Reviews.* **2000,** 173, 17-26.

6. Karp, Gerald. “The Role of NO as an Intracellular Messenger.” Cell and Molecular Biology. 5th ed. John Wiley & Sons. **2008**, 652-653.

7. Boon, E.M., Marletta, M.A. “Ligand specificity of H-NOX domains: From sGC to bacterial NO sensors.” *Journal of Inorganic Biochemistry*. **2005,** 99, 892-902.

8. Boon, E.M., Davis, J.H., Karow, D.S., Huang, S.H., Tran, R.; Miazgowicz, M.M., Mathies, R., Marletta, M.A. “Characterization of NO binding to prokaryotic homologs of the sGC b1 H-NOX domain.” *Journal of Biological Chemistry*. **2006,** 281, 21892-21902.

9. Boon, E.M., Marletta, M.A. “Ligand discrimination in soluble guanylate cyclase and the H-NOX family of heme sensor proteins.” *Current Opinion in Chemical Biolog.* **2005**, 9, 441-446.

10. Boon, E.M., Huang, S.H., Marletta, M.A. “A molecular basis for NO selectivity in soluble guanylate cyclase.” *Nature Chemical Biology*. **2005,** 1, 53-59.

11. Liu, N., Pak, T., Boon, E.M. “Characterization of a diguanylate cyclase from Shewanella woodyi with cyclase and phosphodiesterase activities” *Molecular Biosystems.* **2010,** 6, 1-4.

12. Lee, V.T. *et al.* “A cyclic-di-GMP receptor required for bacterial exopolysaccharide production.” *Mol. Microbiol.* **2007,** 65, 1474-1484.

13. Hickman, J.W., Tifrea, D.F., Harwood, C.S. “A chemosensory system that regulates biofilm formation through modulation of cyclic diguanylate levels.” *Proc. Natl. Acad. Sci. U. S. A.* **2005**, 102, 14422-14427.

14. Tucker, J.M., Oyola, R., Gai, F. “A Novel Fluorescent Probe for Protein Binding and Folding Studies: *p*-Cyano-Phenylalanine.” *Biopolymers.* **2006,** 83, 571-576.

15. Xue, Y., Xu, Y., Liu, Y., Ma, Y., Zhou, P. “*Thermoanaerobacter tengcogensis* sp. nov., A Novel Anaerobic, Saccharolytic, Thermophilic bacterium Isolated From A Hot Spring in Tengcong, China.” *International Journal of Systematic and Evolutionary Microbiology.* **2001,** 51, 1335-1341.

16. Pellicena, P., Karow, D.S., Boon, E.M., Marletta, M.A., Kuri. “Crystal structure of an oxygen-binding heme domain related to soluble guanylate cyclases.” *Proc.Natl.Acad.Sci.Usa*. **2004,** 101**,** 12854-12859.

17. Olea, C., Boon, E.M., Pellicena, P., Kuriyan, J., Marletta, M.A. “Probing the function of heme distortion in the H-NOX family.” *American Chemical Society Chemical Biology.* **2008**, 3, 703-710.

18. Karp, Gerald. “Fluorescence Microscopy (and Related Fluorescence-Based Techniques).” Cell and Molecular Biology. 5th ed. John Wiley & Sons. **2008**, 731-733.

19. Schmidt, I., Steenbakkers, P.J.M., op den Camp, H.J.M., Schmidt, K., Jetten, M.S.M. “Physiologic and Proteomic Evidence for a Role of Nitric Oxide in Biofilm Formation by Nitrosomonas europaea and Other Ammonia Oxidizers.” *Journal of Bacteriology.* **2004,** 186, 9, 2781-2788.

20. Hammill, J.T., Miyake-stoner, S., Hazen, J.L., Jackson, J.C., Mehl, R. “Preparation of Site-Specifically Labeled Fluorinated Proteins for ^{19}F-NMR Structural Characterization.” *Nature Protocols.* **2007**, 2, 10, 2601-2607.

21. *FRET*. Wikipedia, 26 Nov. 2010. Web. 28 Nov. **2010**. <http://en.wikipedia.org/wiki/F%C3%B6rster_resonance_energy_transfer>.

22. Kudla, G., Murray, A.W., Tollervey, D., Plotkin, J.B. “Coding-Sequence Determinants of Gene Expression in *Escherichia coli.*” *Science.* **2009**, 324, 255-258.

23. The PyMOL Molecular Graphics System, Version 1.3r3pre, Schrödinger, LLC.

24. Erbil, W.K., Prince, M.S., Wemmer, D.E., Marletta, M.A. “A structural basis for H-NOX signaling in Shewanella oneidensis by trapping a histidine kinase inhibitory conformation” *PNAS.* **2009,** 16, 47, 19753–19760.

25. Giammona, D.A. **Ph.D. thesis, University of California, Davis (1984)**

26. “2010 AMBER Tutorial with Biotin and Streptavidin” Rizzo, R. 5 May. **2010**. Stony Brook University AMS536. <http://ringo.ams.sunysb.edu/index.php/2010_AMBER _ Tutorial_with_Biotin_and_Streptavidin>

27. Pettersen, E.F., Goddard, T.D., Huang, C.C., Couch, G.S., Greenblatt, D.M., Meng, E.C., Ferrin, T.E. “UCSF Chimera--a visualization system for exploratory research and analysis.” *J Comput Chem.* **2004**, 13,1605-12.

28. D.A. Case, T.A. Darden, T.E. Cheatham, III, C.L. Simmerling, J. Wang, R.E. Duke, R. Luo, M. Crowley, R.C.Walker,W. Zhang, K.M. Merz, B.Wang, S. Hayik, A. Roitberg, G. Seabra, I. Kolossvy, K.F.Wong, F. Paesani, J. Vanicek, X.Wu, S.R. Brozell, T. Steinbrecher, H. Gohlke, L. Yang, C. Tan, J. Mongan, V. Hornak, G. Cui, D.H. Mathews, M.G. Seetin, C. Sagui, V. Babin, and P.A. Kollman (2008), AMBER 10, University of California, San Francisco.

29. Humphrey, W., Dalke, A. and Schulten, K., “VMD - Visual Molecular Dynamics.” *J. Molec. Graphics*, **1996**, 14, 33-38.

30. Hornak, V., Abel, R., Okur, A., Strockbine, B., Simmerling, C. “Comparison of multiple Amber force fields and development of improved protein backbone parameters.” *Proteins*. **2006**, 65, 3, 712-725.

Appendix

I. Gene and Primer sequences

I.1 *Sw*H-NOX Gene (gi: 170727096)

5’ ATG ATG GGC ATG GTT TTC ACA GGG TTA ATG GAG TTG ATT GAA GAT
10

GAG TTC GGA TAT GAA ACC TTA GAT ACT TTA CTT GAG TCA TGT GAG
20 30

TTA CAA AGT GAA GGG ATA TAT ACA TCT GTT GGC AGT TAT GAT CAC
40

CAA GAG TTA CTT CAG TTA GTG GTT AAG CTC AGT GAG GTT TCA TCG
50 60

GTA CCT GTG ACA GAG CTT GTT AGG TTA TTT GGC AAA AAA CTG TTT
70

GTG GAG TTG ATT GAG GGG CAC CCT GAA ATT GCT AAT GAG ATG AAA
80 90

GAC TCT TTC GAT CTG CTT TCT AAA ATA GAC AGC TTT ATT CAT GTG GAG
100

GTT TAT AAG CTT TAT CCT CAA GCC GAA TTA CCC AAA TTT ACC TGT GAT
110 120

CGT TTA GGC GAT AAT GAC ATT AGA CTG CAT TAT CAA TCT AAA AGG
130

CCA TTT GCA TCG TTT GCT GAA GGC TTG CTC GAT GGC TGT GCA GAG
140 150

TAT TTT AAA GAG GAC TTT ACT ATT AGC CGG ACA CCG GAA ACT CAA
160

GAT TCC GAG ACC GAC GTT ATT TTT AAT ATT ACA CGA GCG CCT CGT

TAG 3’

I.2 Cloning Primers

After PCR, these primers produced *Sw*H-NOX amplicons that had a 5' Nco1 site and 3' EcoR1 site. In addition, the stop codon, TAG, was removed. Lastly, these primers were designed to put *Sw*H-NOX in frame with the pBAD/myc-HisC start codon and 6x his-tag after restriction digest and ligation.

Forward: 5'GCCTTA CCATGG GG ATG ATG GGC ATG GTT TTC ACA GGG 3'
Reverse: 5'CGCGTA GAATTC CC ACG AGG CGC TCG 3'

I.3 Site-Directed Mutagenesis Primers

L22W
5' GAT GAG TTC GGA TAT GAA ACC **TGG** GAT ACT TTA CTT GAG TCA TG 3'
5' CA TGA CTC AAG TAA AGT ATC **CCA** GGT TTC ATA TCC GAA CTC ATC3'
V67W
5' CG GTA CCT GTG ACA GAG CTT **TGG** AGG TTA TTT GGC AAA AAA CTG 3'
5' CAG TTT TTT GCC AAA TAA CCT **CCA** AAG CTC TGT CAC AGG TAC CG 3'
F154W
5' GAT GGC TGT GCA GAG TAT **TGG** AAA GAG GAC TTT ACT ATT AGC 3'
5' GCT AAT AGT AAA GTC CTC TTT **CCA** ATA CTC TGC ACA GCC ATC 3'
F70pCN
5'GTG ACA GAG CTT GTT AGG TTA **TAG** GGC AAA AAA CTG TTT GTG GAG 3'
5' CTC CAC AAA CAG TTT TTT GCC **CTA** TAA CCT AAC AAG CTC TGT CAC 3'
H82pCN
5' GTG GAG TTG ATT GAG GGG **TAG** CCT GAA ATT GCT AAT GAG 3'
5' CTC ATT AGC AAT TTC AGG **CTA** CCC CTC AAT CAA CTC CAC 3'
P117A
5' CCT CAA GCC GAA TTA **GCC** AAA TTT ACC TGT GAT CG 3'
5' CG ATC ACA GGT AAA TTT **GGC** TAA TTC GGC TTG AGG 3'
L146W
5' CG TTT GCT GAA GGC **TGG** CTC GAT GGC TGT GC 3'
5' GC ACA GCC ATC GAG **CCA** GCC TTC AGC AAA CG 3'
L146pCN
5' CG TTT GCT GAA GGC **TAG** CTC GAT GGC TGT GC 3'
5' GC ACA GCC ATC GAG **CTA** GCC TTC AGC AAA CG 3'

To reduce the stability of a hairpin close to the ribosome binding site
5' GG GCT AAC AGG AGG AAT **ATT** CCA TGG GGA TGA TGG GC 3'
3' CC CCA TCA TCC CCA TGG **AAT** ATT CCT CCT GTT AGC CC 5'

II. List of Mutations Made in *Sw*H-NOX

P117A
H82pCN
F70pCN
L146pCN
H82pCN V67W
H82pCN V67W P117A
L146pCN V67W
L146pCN L22W
L146pCN V67W P117A
L146pCN L22W P117A
F70pCN L146W
F70pCN F154W
F70pCN L146W P117A
F70pCN F154W P117A
H82pCN P117A
F70pCN P117A
L146pCN P117A
L146W
F154W
L22W
V67W
L146W P117A
F154W P117A
L22W P117A
V67W P117A